
Automated Microburst Wind-Shear Prediction

Marilyn M. Wolfson, Richard L. Delanoy, Barbara E. Forman,
Robert G. Hallowell, Margita L. Pawlak, and Peter D. Smith

■ We have developed an algorithm that automatically and reliably predicts microburst wind shear. The algorithm, developed as part of the FAA Integrated Terminal Weather System (ITWS), can provide warnings several minutes in advance of hazardous low-altitude wind-shear conditions. Our approach to the algorithm emphasizes fundamental principles of thunderstorm evolution and downdraft development and incorporates heuristic and statistical methods as needed for refinement. In the algorithm, machine-intelligent image processing and data-fusion techniques are applied to Doppler radar data to detect those regions of growing thunderstorms and intensifying downdrafts which lead to microbursts. The algorithm then uses measurements of the ambient temperature/humidity structure in the atmosphere to aid in predicting a microburst's peak outflow strength. The algorithm has been tested in real time as part of the ITWS operational test and evaluation at Memphis, Tennessee, and Orlando, Florida, in 1994.

MICROBURSTS BEGIN AS small powerful downdrafts, typically inside thunderstorms, that descend from 3000 to 6000 m above ground level. When these cold downward rushes of air reach the ground, they spread out, or burst, horizontally in all directions, creating a locally intense divergent wind shear that is very shallow (Figure 1). When an aircraft encounters this wind pattern, which often develops quite suddenly (within one to two minutes), the aircraft first experiences a headwind, which actually serves to increase the flow of air over the wings, thus increasing the lift. If the pilot is trying to approach on the glide slope, the pilot may attempt to correct for this lift by bringing the aircraft's nose downward so as not to overshoot the runway. Immediately after encountering the headwind, though, the aircraft experiences a downdraft, which forces the plane downward. Finally, the aircraft encounters a strong tailwind, which reduces the net airflow over the wings, thus reducing the lift. Because this divergent wind pattern is encountered near the ground, the aircraft has little or no room to descend

before recovering airspeed and flying out of the microburst [1].

There is little debate that microbursts are the most serious wind hazard in aviation. According to the National Transportation Safety Board (NTSB), thunderstorm outflow or microburst wind shear has caused 21 aircraft accidents in the United States since 1975, killing 438 people (Table 1). The most recent accident attributed to wind shear occurred on 2 July 1994 in Charlotte, North Carolina.

Research in the late 1970s and early 1980s demonstrated that Doppler weather radars could reliably measure the divergent wind pattern associated with microbursts [2, 3]. Thus the FAA began the Terminal Doppler Weather Radar (TDWR) program in 1983 to develop a system that could provide wind-shear and microburst warnings to air traffic controllers and pilots in the terminal area [4, 5]. Forty-seven TDWR systems have been purchased under the program, and approximately twenty of those systems were on site and operating by the end of 1994 [6].

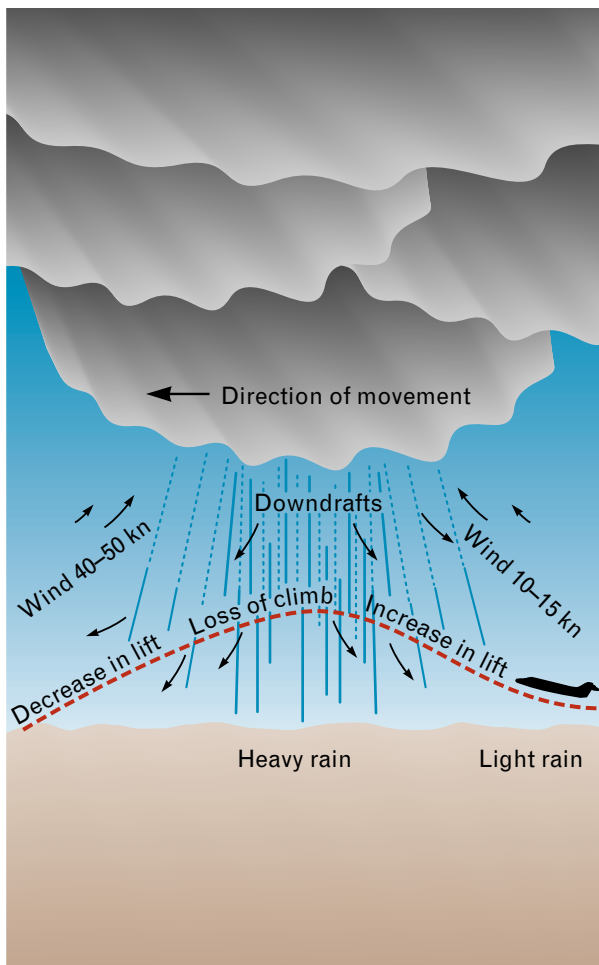
Although TDWR can provide highly reliable mi-

icroburst warnings, there still remains a period of time between microburst onset and pilot reaction during which aircraft are at risk. This delay results from the time needed for the radar to scan the area, the computer algorithms to generate detections, the system to relay warnings to pilots, and the pilots to react to the warnings. In other words, a hazardous situation may exist prior to pilot action. Figure 2 shows an example of a microburst encounter at Orlando, Florida, that occurred even though a prototype TDWR testbed was operating and supplying wind-shear and microburst alerts. The graph shows that, during just one

minute, the loss of relative airspeed on the runway increased from wind-shear levels (15 to 25 kn) to well above the microburst threshold (30 kn). The aircraft shown in red was already encountering the microburst-strength loss when the alert was read over the radio. Prior radio reports had indicated that the wind shear was decreasing in strength when, in fact, the wind shear was about to increase. In general, earlier warnings would decrease any delays and enable pilots to commence avoidance procedures earlier, thus increasing the margin of safety.

Our research has resulted in the development of an

FIGURE 1. Downdrafts from a thunderstorm can be hazardous to an airplane during takeoff or landing: (below) schematic of a pilot taking off in a microburst, and (right) photograph of a microburst-producing thunderstorm in Orlando, Florida. The pilot first encounters a headwind (increase in lift), then a downdraft (loss of climb), and, finally, a tailwind (decrease in lift), which causes the airplane to lose airspeed.



algorithm that automatically and reliably *predicts* microburst wind shear, and provides several minutes of lead time before hazardous low-altitude wind-shear conditions arise. This work is part of the FAA Integrated Terminal Weather System (ITWS) being developed at Lincoln Laboratory [7]. In this article we describe characteristics of the microburst phenomenon and our approach to solving the microburst prediction problem. We then provide a description of the algorithm developed and the results of live demonstrations of the algorithm in Memphis, Tennessee, and Orlando in 1994.

Characteristics of Microburst Storms

From 1984 through 1993, Lincoln Laboratory operated a testbed prototype of the TDWR system at several locations: Memphis (1984–1985); Huntsville, Alabama (1986); Denver, Colorado (1987–1988); Kansas City, Missouri (1989); and Orlando (1990–1993). The tests provided the most extensive collection of microburst data available in the meteorological research community, with examples ranging from wet microbursts (i.e., microbursts associated with very heavy rain) in the humid Southeast environment

Table 1. Aircraft Accidents in the United States Attributed to Thunderstorm Outflow or Microburst Wind Shear in the Past Twenty Years (1975–1994)

<i>Date</i>	<i>Location</i>	<i>Aircraft</i>	<i>Fatalities</i>	<i>Injuries</i>	<i>Uninjured</i>
24 June 1975	Jamaica, NY	Boeing 727	112	12	0
7 Aug. 1975	Denver, CO	Boeing 727	0	15	119
23 June 1976	Philadelphia, PA	McDonnell-Douglas DC-9	0	86	20
3 June 1977	Tucson, AZ	Boeing 727	0	0	91
21 May 1982	Dayton, OH	BAC 1-11	0	0	48
9 July 1982	New Orleans, LA	Boeing 727	153	9	7
28 July 1982	Flushing, NY	Boeing 727	0	0	129
31 May 1984	Denver, CO	Boeing 727	0	0	105
13 June 1984	Detroit, MI	McDonnell-Douglas DC-9	0	10	46
2 Aug. 1985	Dallas/Ft. Worth, TX	Lockheed L-1011	135	28	2
11 July 1987	Washington, DC	Boeing 727	0	0	87
15 Sept. 1987	Tulsa, OK	Boeing 727	0	0	62
3 Nov. 1987	Orlando, FL	Lear Jet 35A	0	0	5
1 June 1988	Jamaica, NY	Boeing 747	0	0	157
26 Apr. 1989	Mt. Zion, IL	Cessna 208A	0	1	0
22 Nov. 1989	Beaumont, TX	Saab-Fairchild 340A	0	0	37
18 Feb. 1991	Thornton, TX	Cessna 172N	1	0	0
14 Feb. 1992	Lanai, HI	Beech D-18H	0	0	1
7 Jan. 1993	Akutan, AK	Grumman G-21A	0	0	8
26 Apr. 1993	Denver, CO	McDonnell-Douglas DC-9	0	0	90
2 July 1994	Charlotte, NC	McDonnell-Douglas DC-9	37	20	0

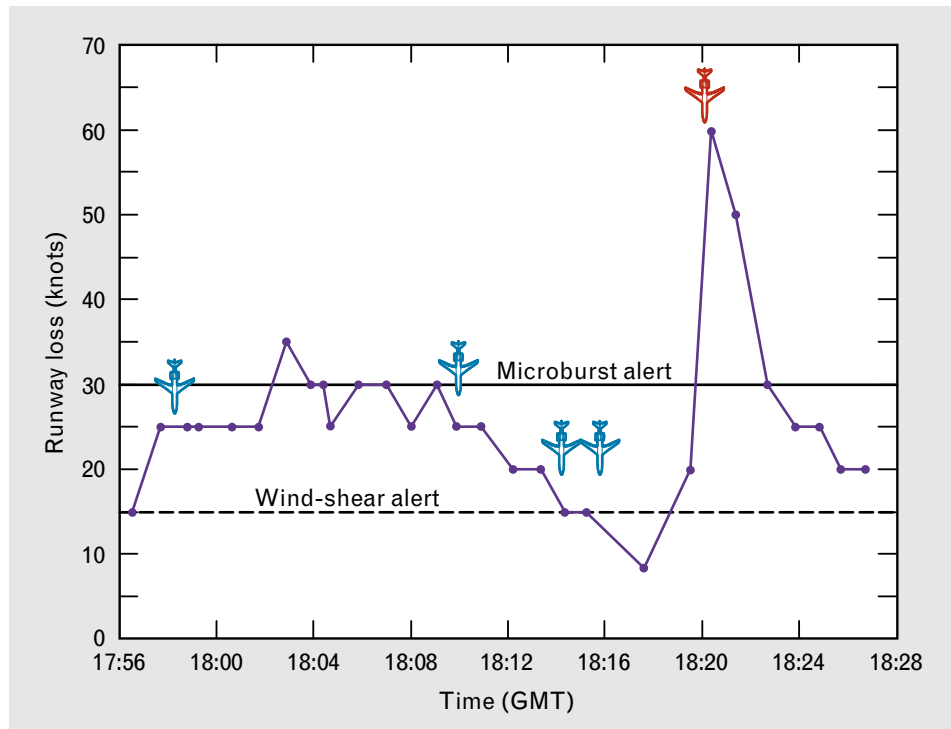


FIGURE 2. Five aircraft landed at Orlando International Airport (MCO) between 17:56 and 18:24 (Greenwich mean time [GMT]) on 27 May 1992. For that period, the purple curve shows the runway loss, i.e., the loss of relative airspeed on the runway. This runway loss would be experienced by an aircraft that was landing or taking off. The aircraft shown in blue all encountered wind shear less than 30 kn. The aircraft shown in red unintentionally encountered microburst-strength wind shear greater than 30 kn.

to dry microbursts (i.e., microbursts associated with almost no measurable surface rainfall) in the semiarid environment of the High Plains near the Rocky Mountains [8–10].

In studying these storms, many researchers speculated about the forcing mechanisms that are responsible for microbursts. If these mechanisms could be identified and quantified, then prospects for reliable predictions would be promising. Some researchers argued that, because radar reflectivity is proportional to water content, which is proportional to downward vertical acceleration, there should be a monotonic relationship between downdraft/outflow strength and reflectivity. We have found, however, that storms with similar reflectivity signatures can, on different days, produce outflows of very different strengths. Furthermore, storms with very different reflectivity levels can, on different days, produce very similar outflows. Figure 3 shows that, although the surface reflectivity of a wet Orlando microburst and a dry Denver mi-

croburst are extremely different, the corresponding Doppler velocity patterns of their divergent outflows are quite similar. Reflectivity differences are caused by environmental factors, such as the temperature and humidity structure in the atmosphere, that determine the degree of melting of frozen precipitation and the degree of evaporation of rain. Such thermodynamic effects chill the downdraft air, and also cause the air to accelerate downward and then outward when it hits the ground. Because water phase changes are usually not observable with Doppler weather radars, we recognized at the outset of our research that explicit consideration of the atmospheric temperature and humidity profile was necessary for reliable microburst prediction.

The most detailed datasets for studying the evolution of microburst-producing thunderstorms were collected in Orlando from June through September 1991 [11]. During that period, the FAA sponsored the coordinated collection of data from three C-band

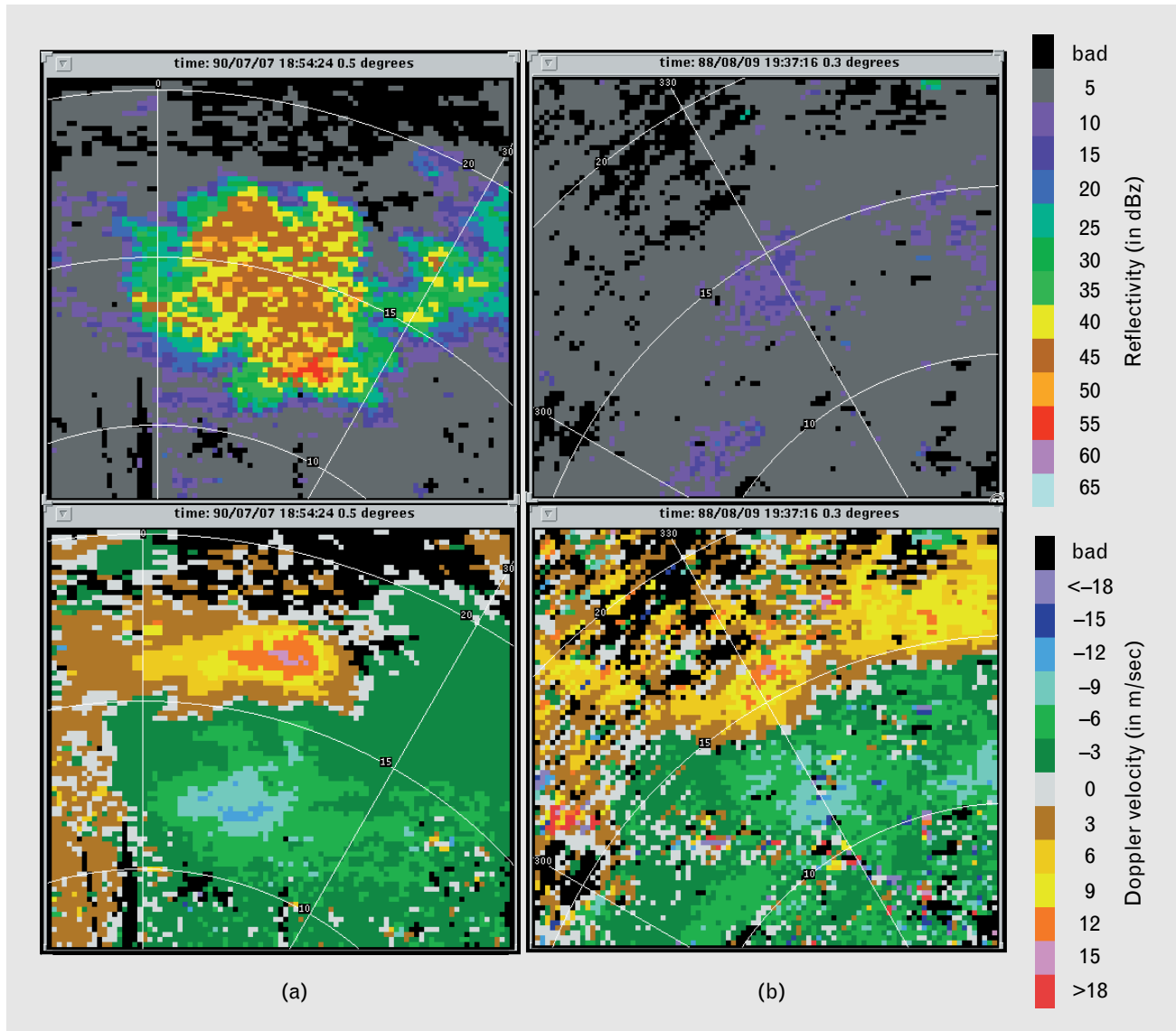


FIGURE 3. Comparison of two microbursts: (a) a wet microburst in Orlando on 7 July 1990, and (b) a dry microburst in Denver on 9 August 1988. The top images are for the reflectivity at the ground surface and the bottom images are for the Doppler velocity. The Orlando microburst has high reflectivity and heavy rain; the Denver microburst has very low reflectivity and little or no rain. Note, though, how similar the Doppler velocity patterns are for the two storms.

Doppler weather radars: the TDWR testbed radar, the University of North Dakota radar, and the MIT radar (Figure 4). Because a Doppler radar can measure only one component of the wind (motion toward or away from the radar), wind measurements from a single Doppler radar are ambiguous. If, however, three Doppler radars are used to scan the same airspace simultaneously, the full three-dimensional wind field can potentially be reconstructed. Our three-radar configuration and new wind-synthesis

technique developed especially for use with this network allowed the determination of the wind velocity with errors of only 1 to 2 m/sec within the triangle defined by the three radars [12].

In researching the microburst-prediction problem, we examined thunderstorms through all stages of their life cycles to discern commonalities and reliable discriminating features that could be used in an automated algorithm. We studied microburst phenomena also to determine the optimal type of algorithm de-

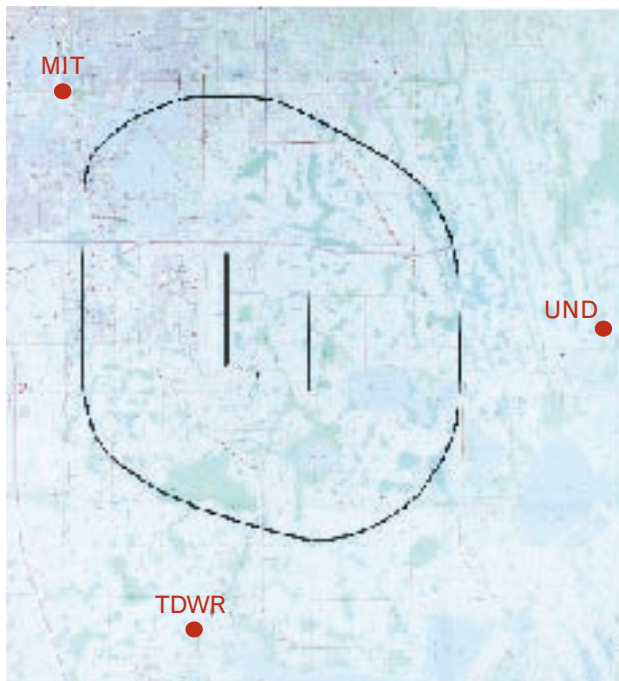


FIGURE 4. Map showing the locations of the three radars used to collect data on microburst-producing thunderstorms in Orlando from June through September 1991. The three C-band radars are the Terminal Doppler Weather Radar (TDWR) testbed system, the University of North Dakota (UND) radar, and the MIT radar. Runways for the Orlando International Airport are shown as three north-south oriented lines near the center of the map. The black curve that encircles the runways indicates a distance 3 nmi away from the runways. The area near the airport, at the center of the triangle defined by the three Doppler radars, is the most favorable for the determination of the three-dimensional wind field.

sign. Statistics were gathered on a large number of thunderstorms, both those that did produce microburst wind shear and those that did not.

The strongest microburst recorded in Orlando in 1991 had a wind-shear differential of 90 kn. This microburst occurred on 9 August near the center of our network of three Doppler radars. As the thunderstorm propagated very slowly from west to east, we recorded data on the full life cycle of many cells in that multicell storm. Each of the three radars scanned a pattern of evenly spaced beams up to an elevation of 60° for an azimuth sector roughly 120° wide directed toward the center of the triangle. Each time-coordinated volume scan took 3 min to complete.

Figure 5 shows a vertical cross section through

the evolving thunderstorm along the direction of propagation. The growing cell at the right of the cross section is filled with updraft (Figure 5[a]), and the cell's reflectivity increases until it reaches a peak greater than 60 dBz at about 7 km above ground level (AGL) (Figure 5[b]). The water mass then becomes too heavy for the updraft to support, and a downdraft develops through the center of the cell (Figure 5[c]). Meanwhile, air is still moving upward at all altitudes on the leading edge (right side) of the cell. The top of the storm accelerates upward at this time because the updraft in the upper portions of the cell has shed the water that was weighing it down. Finally, downdraft has filled the entire bottom half of the cell and a microburst outflow takes place at the ground surface (Figure 5[d]). In addition to the growing storm cell at the right of the cross section in Figure 5(a), there was a storm to the left that was filled with downdraft, which also produced a microburst. Note that the reflectivity for this storm steadily decreases over the four-frame series. This example illustrates the classic pattern of multicell thunderstorm evolution.

In 1946 through 1947, after the end of World War II, H.R. Byers and R.R. Braham, Jr., conducted the Thunderstorm Project [13] to investigate "the weather hazard that had caused many serious accidents to commercial and military aircraft." In their final report, which is still read today as an excellent introduction to thunderstorm phenomenology, Byers and Braham divided the life cycle of a thunderstorm cell into three stages:

1. the cumulus stage, characterized by updraft throughout the cell,
2. the mature stage, characterized by the presence of both updrafts and downdrafts at least in the lower half of the cell, and
3. the dissipating stage, characterized by weak downdrafts prevailing throughout the cell.

In our example, the growing cell at the right in Figure 5 is in the cumulus stage in parts *a* and *b*, and in the mature stage in parts *c* and *d*. The decaying cell at the left of the figure is in the mature stage in part *a*, and in the dissipating stage in all subsequent frames. The most important stages for predicting microbursts are the cumulus stage, when the cell

grows rapidly and reflectivity increases, and the beginning of the mature stage, when the downdraft begins to develop at upper levels in the cell. Once downdraft has filled the cell and rain has begun to reach the ground, the microburst is essentially in progress and no warning lead time is possible.

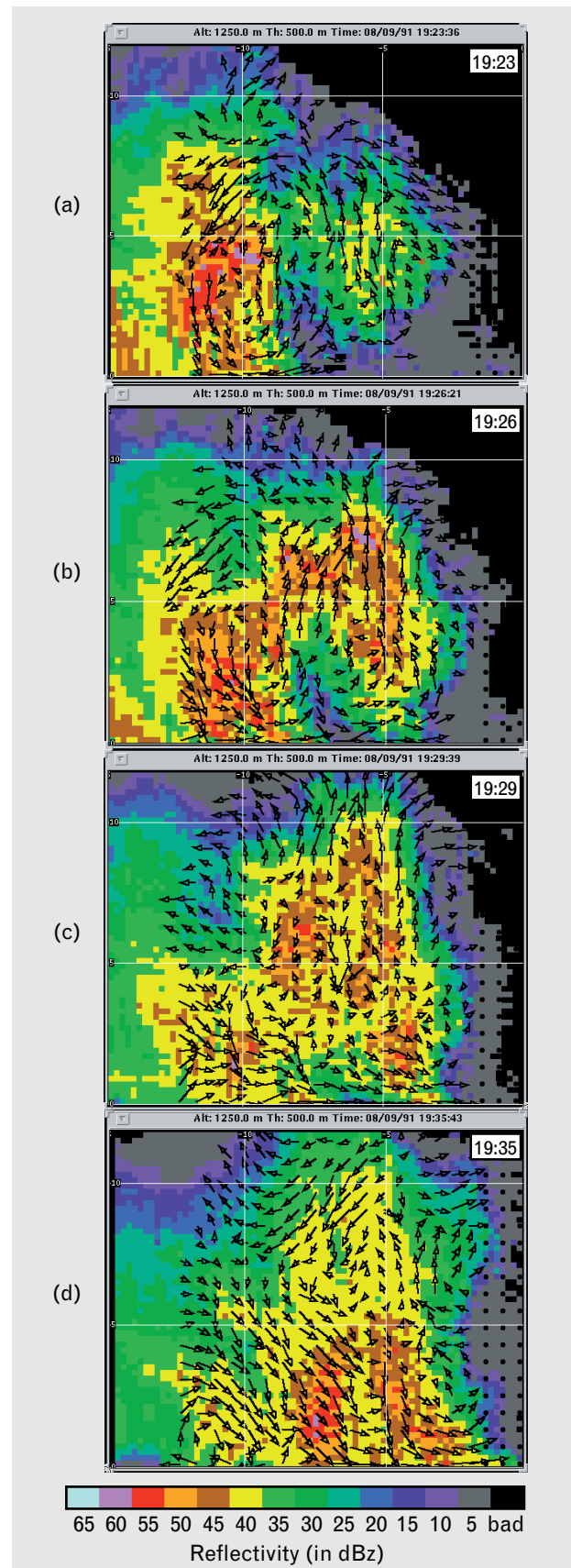
Approach

The research results discussed in the previous section were available when we began developing the ITWS Microburst Prediction Algorithm in the fall of 1991. Yet much work remained to be done to choose and develop effective automated processing methods for analyzing the stages of storm life cycles. In this section, we discuss our approach to designing the algorithm.

Identifying Thunderstorm Cells

Although human analysts of weather radar data can identify thunderstorm cells rather easily, the task is challenging for automated systems. Nonetheless, the automatic identification of storm cells would intuitively appear to be the first step in building an algorithm for predicting microbursts. Almost all systems that are designed to track and quantify characteristics of storms throughout their life cycles have identified *cells* as regions above a certain (perhaps adaptive) reflectivity threshold [14–17]. Figure 6 schematically illustrates this approach of using a threshold to define storm cells. In the approach, each radial of radar data is processed to locate reflectivity above a certain threshold (e.g., 40 dBz). The resulting above-thresh-

FIGURE 5. Vertical cross sections taken at different times along the direction of motion of a thunderstorm complex in Orlando. The thunderstorm complex, which occurred on 9 August 1991, produced the strongest microbursts recorded in Orlando that year. In frame *a*, the storm at left is collapsing (downdraft), while the storm at right is just beginning to grow (updraft). In frame *b*, the right storm has increased in size and is still filled with updraft. Later, in frame *c*, the right storm has matured and is filled with updraft (at the right) and downdraft (in the center). Lastly, in frame *d*, the lower portion of the right storm is filled with downdraft and the microburst outflow is at full strength at the ground surface. Note that, during this same four-frame period, the reflectivity for the storm at the left has decreased steadily.



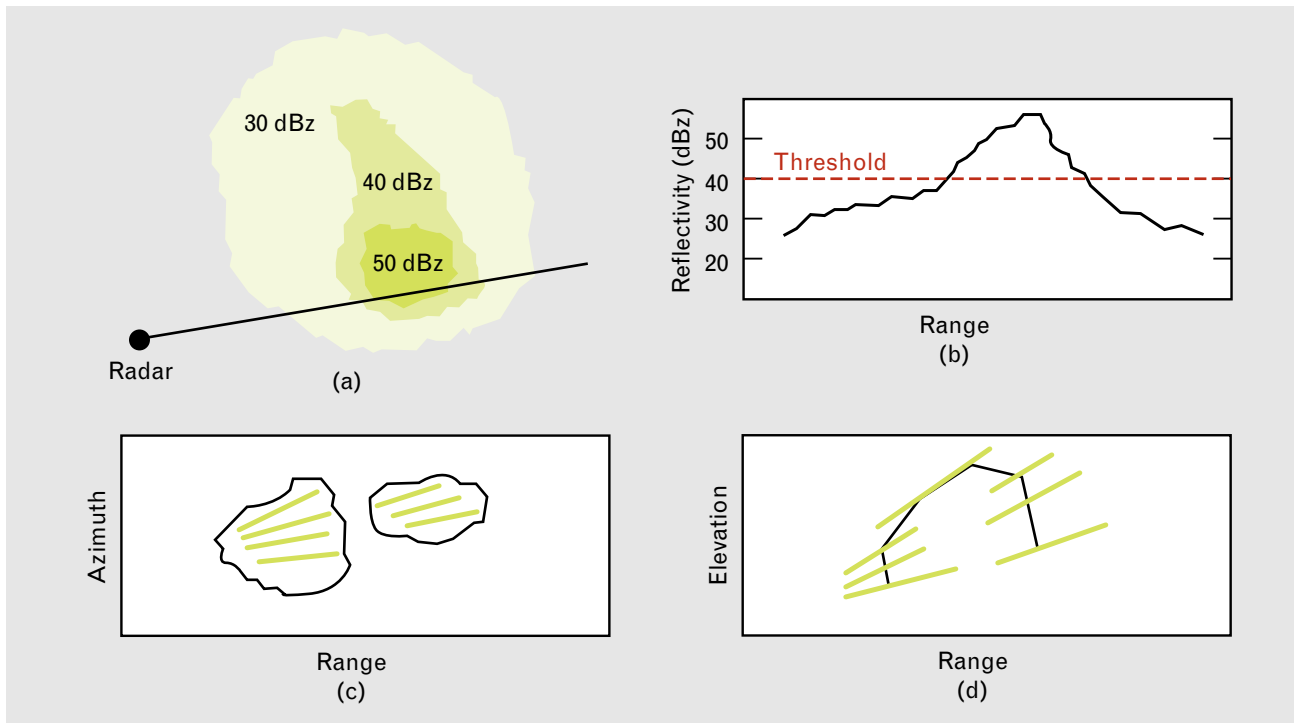


FIGURE 6. Schematic illustrating the segment-based approach to locating storm cells: (a) a radar scans a storm cell, (b) each radial of radar data is processed to locate reflectivity above a certain threshold (e.g., 40 dBz), (c) radial segments above this threshold are grouped together in clusters, and (d) the clusters are associated with one another vertically to build up a storm object. Although this example is shown in radar-centric spherical geometry, the process is identical in a Cartesian geometry.

old segments are grouped into clusters, and the clusters are connected vertically to build up a storm object.

Unfortunately, cells (as defined by these regions located with thresholds) merge and split as the storms undergo their natural cycle of increasing then decreasing reflectivity. This merging is illustrated in Figure 6(d), in which the process of associating grouped segments vertically has resulted in the connecting of two distinct storm regions. In Figure 5(b), the decaying storm on the left and the growing storm on the right are bridged at the 40-to-50-dBz level. Most automated cell-defining techniques that use reflectivity thresholds would merge this entire region and the results would be ambiguous regarding whether the single “cell” was growing or decaying.

We recognized that the reflectivity-threshold approach to cell finding is fundamentally misleading in that storm cells are not defined by reflectivity regions (although reflectivity certainly reveals the presence of storm cells). Actually, thunderstorm cells are unstable

regions of the moist atmosphere that undergo rapid thermodynamic phase changes such as condensation and evaporation. These phase changes lead to strong vertical air motions—in fact, there is a regular progression of each unstable region through the life-cycle stages of thunderstorm evolution—and the result of this strong vertical overturning is a restoration of atmospheric stability. Thus a new methodology was needed to develop a reliable algorithm for microburst prediction. In the new methodology, cells would be identified not as reflectivity regions determined by thresholds but as regions that exhibit properties of growth (updraft and condensation) and subsequent decay (downdraft and evaporation).

At Lincoln Laboratory, ongoing efforts in developing automatic target recognition (ATR) systems ultimately provided this new methodology [18]. Techniques of low-level machine intelligence have been utilized very effectively not only for traditional applications, such as the detection of military ground vehicles, but also for the identification of

meteorological targets such as gust fronts [19]. A similar system, discussed in more detail later in this article, forms the image-processing portion of the ITWS Microburst Prediction Algorithm.

Detecting Microburst Precursors

Since the beginning of TDWR algorithm development, researchers realized the importance of detecting precursors to microbursts so that warnings could be issued in a timely fashion. The TDWR scan strategy was designed for just this purpose with complete coverage of a specified volume of airspace (a sweep of 120° in azimuth at elevation angles from 0.2° up to 40°–60°) every 2 to 3 min during significant weather events near the airport. M.W. Merritt et al. [5] have described the detection of *features aloft* that precede the surface outflow development by 5 to 10 min. These features include the existence of a reflectivity core (i.e., a region of concentrated high reflectivity), high-altitude Doppler velocity features such as the convergence of wind velocities (associated with the inflow of air as the reflectivity core descends), and vorticity (which often develops with velocity convergence) [20]. Any precursor model that is based only on radar data will suffer some inaccuracy because important environmental characteristics must also be considered. Furthermore, there have been problems with identifying the TDWR reflectivity core (a traditional approach of applying thresholds has been used) and with detecting Doppler velocity features aloft (horizontal and vertical motions could not be distinguished unambiguously).

Initially, we decided to focus on only those features of thunderstorm evolution which are extremely reliable, i.e., features that can be expected in essentially every cell. These features include the growth and subsequent decay of the reflectivity field, but do not include the Doppler velocity features, which are ambiguous and not nearly as reliable as the reflectivity features. In addition, the processing required to detect Doppler velocity features would have increased the computational expense of the algorithm.

To assess the growth in reflectivity, we studied a very useful quantity in radar image processing called the vertically integrated liquid water (VIL), which is obtained in the following way. The water content of a

volume of airspace is calculated directly from the radar reflectivity with the use of an assumed or measured distribution of raindrop sizes. This water equivalent of reflectivity is then converted from polar to Cartesian coordinates in three dimensions, and summed vertically to obtain VIL. Note that the use of VIL greatly simplifies the algorithmic processing by reducing a full three-dimensional view of the condensed water in the atmosphere to a two-dimensional plane.

To assess the descent of the reflectivity core and the development of downdraft, we investigated trends in the storm center of mass (CM). The storm CM is computed by again converting radar reflectivity to water content, converting the data from polar to Cartesian coordinates in three dimensions, and then finding the mass-weighted center in each column of data. These altitude values can be mapped in two dimensions to make a two-dimensional image of CM.

Figure 7 (top) illustrates a classic case of thunderstorm evolution as seen by a TDWR system in Orlando on 14 July 1994 for a storm that was only 10 km away from the radar. Note that the TDWR resolution and vertical coverage are outstanding.

The two-dimensional pixel values of VIL and CM were each averaged to obtain the single values plotted in Figure 7 (bottom). Note that VIL increases monotonically with time until reaching its peak at 20:39, and then decreases rapidly before leveling off. CM changes little initially, but then decreases rapidly between 20:37 and 20:42. This drop-off occurs approximately 10 min before the outflow differential velocity (ΔV) reaches microburst strength (15 m/sec, or 30 kn). These measurements, and similar evidence from many other storms, reveal that a drop in CM in the same region that has previously undergone a growth in VIL is indicative of a downdraft associated with the collapse of the cell. After the cell collapses, both CM and VIL then level off for a short time before a strong outflow begins (in Figure 7 [bottom], the outflow begins to increase dramatically after 20:46). This time lapse can be thought of as a transition period when neither VIL nor CM is changing much, and the downdraft is just beginning to reach the ground and initiate the outflow.

Using this type of analysis, we have identified three

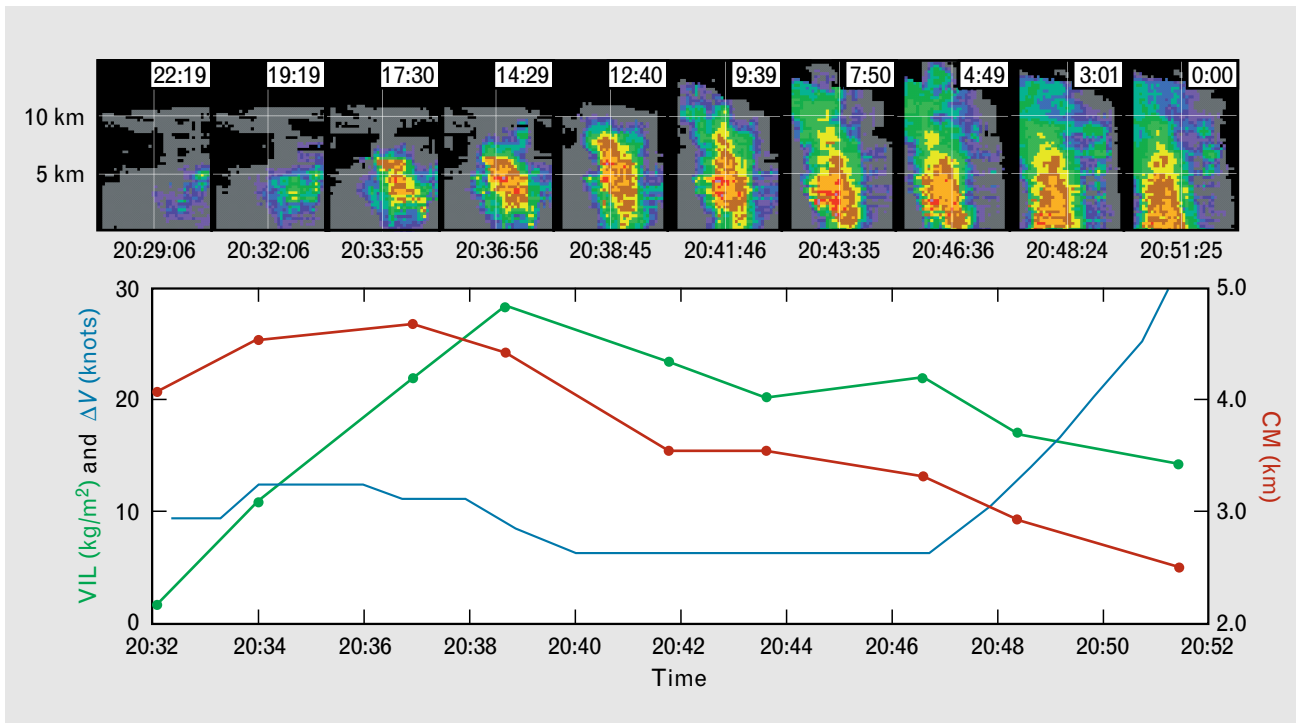


FIGURE 7. An evolving thunderstorm that occurred in Orlando on 14 July 1994: (top) radar vertical cross sections with the time to microburst onset listed at the top of each frame, and (bottom) measurements of the vertically integrated liquid water (VIL), shown in green; the height of the center of mass (CM), shown in red; and the speed of the microburst differential outflow (ΔV), shown in blue; as a function of time for the cells shown at the top. Each data point represents an average for the cell at that time. Note that VIL increases monotonically, and that CM changes little at first but then drops rapidly after VIL has peaked. These changes are precursors to the microburst, which does not occur until the very end of the frame sequence. These data were collected with an FAA operational TDWR system that was installed in the spring of 1994.

stages of storm evolution that can be used for the reliable prediction of microbursts. The stages, which are directly related to observable radar features, are defined as

1. growth, which is characterized by an increase in VIL (this precursor occurs first and thus provides the best hope for long prediction lead times),
2. downdraft, which is characterized by an overall drop in the CM in a region, and
3. transition, which is characterized by regions that had previously exhibited downdraft features and that are just beginning to show surface outflow characteristics.

These stages provide the basis for categories of *feature detectors*—computational modules that have been designed specifically to detect each of the above characteristics. Used in the ITWS Microburst

Prediction Algorithm, the GROWTH, DOWNDRAFT, and TRANSITION feature detectors are described in greater detail later in this article.

Estimating Microburst Outflow Strength

Another key problem in predicting microbursts is estimating the strength of a thunderstorm downdraft to determine if it will be strong enough to produce an outflow with a differential velocity greater than the microburst threshold of 30 kn. Research has shown that this estimation is possible by using the vertical-momentum equation to indicate the expected dependence of the vertical velocity w on the various mechanisms at work in the thunderstorm downdraft [21–23]:

$$\frac{dw}{dt} = g \frac{T_d - T_e}{T_e} - g(L + I) + f_{\text{pressure}} \quad (1)$$

The term on the left side of Equation 1 represents the vertical acceleration (e.g., in a thunderstorm downdraft), and the terms on the right side represent the physical processes forcing the downdraft. From left to right, these processes are the buoyancy forcing (g is the gravitational acceleration and T_d and T_e are the temperature of the air in the downdraft and environment, respectively), the water loading (L and I are the mass of liquid water and ice, respectively, per unit mass of air), and the last term represents the effects of pressure forces that, as the downdraft reaches the ground, decelerate the downdraft and accelerate the outflow.

Our strategy in developing a downdraft/outflow strength estimator was to relate each term in Equation 1 to the observable environmental or storm characteristic that is physically responsible for the term's ultimate magnitude. The vertical acceleration can be related directly to the vertical velocity and the height of the freezing level because the bulk of the evaporative cooling in the downdraft takes place below this level. The buoyancy forcing can be related to the temperature lapse rate, i.e., the rate of change of temperature with height in the environment. The water loading can be related to the radar-measured reflectivity with the use of a selected or default distribution of raindrop sizes. The downdraft-induced pressure forces depend on the size and strength of the downdraft. These forces ultimately drive the divergent outflow as the downdraft reaches the ground. In addition to these pressure forces, the outflow velocity also depends on the temperature of the downdraft air.

By coupling our estimated prediction of the downdraft velocity from Equation 1 with the equation for mass continuity, we obtain the final equation for outflow speed [21]:

$$\text{outflow} = a\gamma\sqrt{b\gamma F[c\gamma + (c_{f,b}VIL)^{3/2} - c_f]}, \quad (2)$$

where a , b , and c are empirical coefficients, γ is the temperature lapse rate from the ground surface to the freezing level, F is the freezing level, VIL is the vertically integrated liquid water, and c_f is a forcing constant that represents the minimum amount of forcing needed in any storm to initiate a downdraft. Described later in this article, $c_{f,b}$ is a feedback coefficient

that allows the equation to be adjusted on the basis of a comparison of actual microburst detections with predictions. Initially, $c_{f,b}$ is set to 1.

An unstable situation can arise when the lapse rate γ is large and Equation 2 predicts an outflow of microburst strength even when $VIL = 0$, i.e., even when no storm is present. Recognizing when this situation has occurred and automatically taking the appropriate action can prevent serious false alarms. There are other situations in which γ is small and even a large VIL cannot make the radicand in Equation 2 positive. In these cases, we set the outflow equal to zero, meaning that there is no possibility that microburst wind shear will occur.

Design of the Microburst Prediction Algorithm

A high-level block diagram of the ITWS Microburst Prediction Algorithm is shown in Figure 8. The algorithm consists of several different components, and utilizes two other ITWS algorithms—Storm Motion and Microburst Detection—in its operations. The following subsections describe each of the different components in greater detail.

Sounding Generator

A key component of the ITWS Microburst Prediction Algorithm is the Sounding Generator, which creates a vertical profile of temperature and humidity in real time. The humidity data are used to adjust the temperature data to compute a modified air density called the *virtual temperature*, and the constructed profile is used to estimate the height of the freezing level and the lapse rate from the ground surface to the freezing level. These parameters are used in Equation 2 to estimate the microburst outflow strength. The equation is also used implicitly in detecting the downdraft because many of the feature detectors have the underlying notion that, for a given sounding, a minimum amount of VIL is necessary to produce a microburst. Thus we need to estimate the soundings as accurately as possible.

The Sounding Generator uses several different sources of data. One source is supplied by the rawinsondes (sounding balloons) that are launched daily by the National Weather Service at 0:00 and 12:00 Greenwich mean time (GMT) to measure the tem-

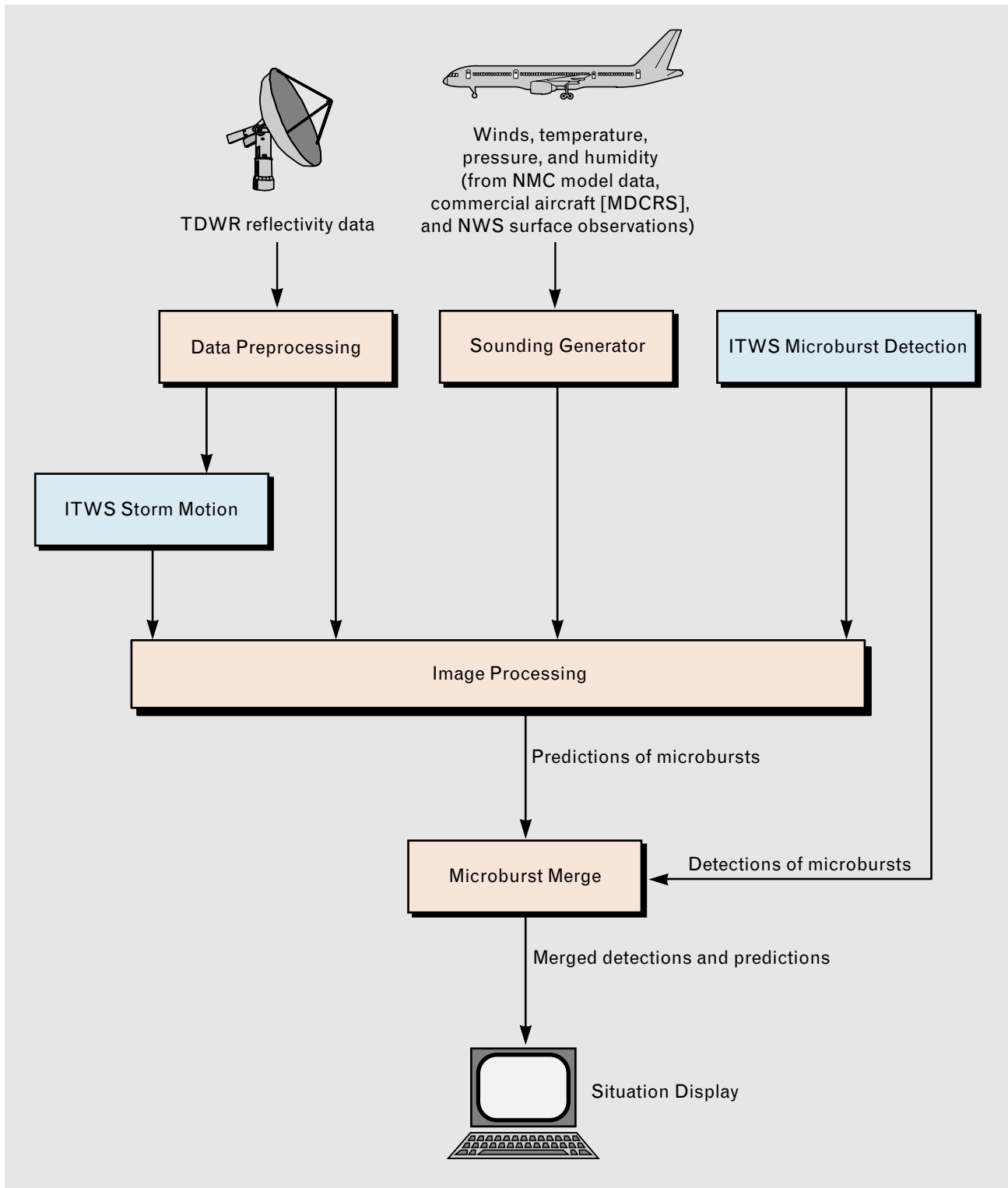


FIGURE 8. The ITWS Microburst Prediction Algorithm (shown in red). At the top are the various input data sources, including the TDWR, the National Meteorological Center (NMC), the Meteorological Data Collection and Reporting Service (MDCRS), and the National Weather Service (NWS). Note that the results of other ITWS algorithms (shown in blue) are used by the Microburst Prediction Algorithm. At the bottom of the figure, the Microburst Merge component combines predictions and detections into one information stream for viewing on a Situation Display.

perature, humidity, and winds as a function of the height above ground. These data are interpolated to a Cartesian grid at the National Meteorological Center (NMC). The data are then made available in combination with other data as part of the NMC's objective analysis. The analyses are used to initialize numerical weather prediction models, and the predictions from these models provide a key data source for the Sounding Generator. From NMC's Rapid Update Cycle model (hourly forecasts out to 12 hr updated every 3 hr [24]), we choose the single grid point that is nearest the airport and include this column of data in our composite sounding.

Another source of data to the Sounding Generator is supplied by the Meteorological Data Collection and Reporting System (MDCRS) [25]. Every 5 to 7 min, commercial aircraft record measurements of winds and temperature both en route and during ascent and descent in the terminal area. These measurements are bundled together and transmitted via a VHF radio communication system approximately every 45 min. MDCRS packages aircraft meteorological data from each participating airline into a common format, and makes the data available to the FAA and to NMC for inclusion in its model's analyses [26]. When a sufficient number of reports are available, these data have an enormous impact on the accuracy of our generated soundings. Future improvements to this data source include adding humidity measurements by installing humidity sensors on aircraft [27], adding more airlines, and increasing the reporting frequency (especially in ascent and descent mode) to obtain accurate soundings in the terminal area. (Note: Originated by Aeronautical Radio, Inc. [ARINC], MDCRS utilizes the ARINC Communications, Addressing and Reporting Service [ACARS] to provide air-to-ground communications.)

Other sounding data sources include surface observations made hourly by the National Weather Service (NWS) and more frequently (every 5 min) by the Automated Surface Observation System (ASOS). The ASOS data includes measurements of temperature, humidity, winds, pressure, and rainfall.

Figure 9 illustrates the generation of a temperature sounding from actual data taken on 5 August 1992 at 19:00 GMT in Orlando. The data have been weight-

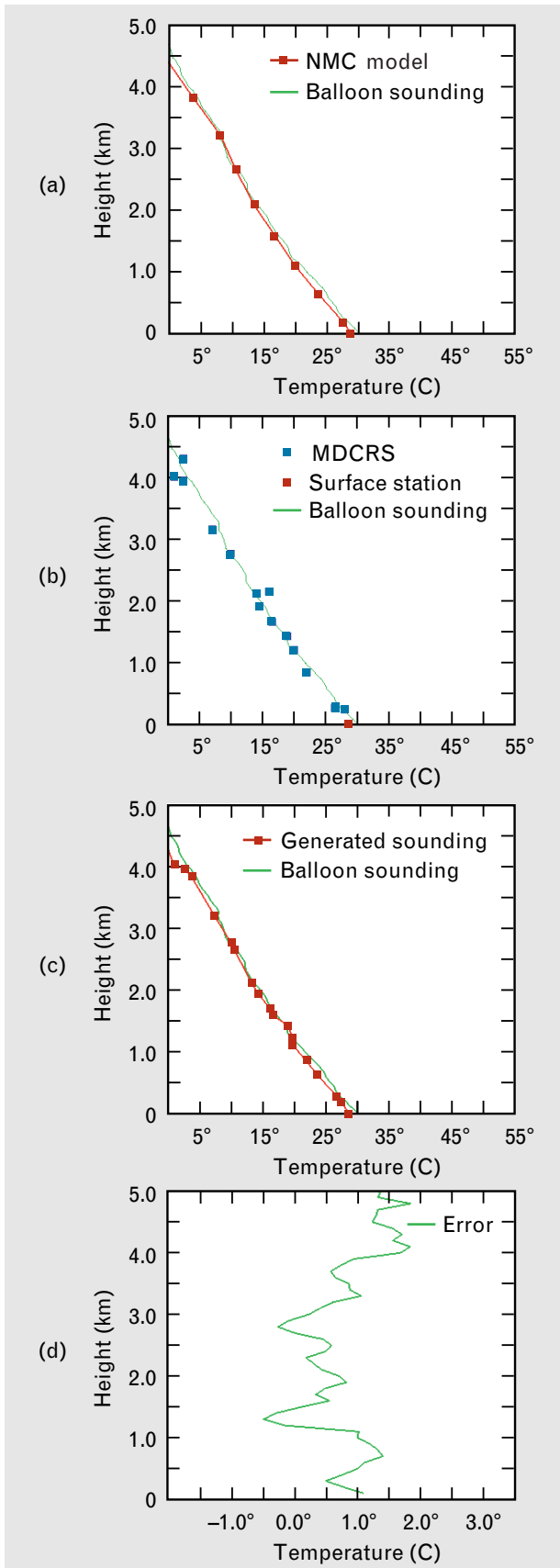
ed linearly in space and time: surface data have been weighted linearly out to a maximum distance of 25 km and maximum time of 3 hr; upper-air data have been weighted linearly out to 100 km and 6 hr. Because meteorological variables can vary rapidly in the vertical direction, a distance *influence* of only 50 m has been assigned; i.e., for a given data point, only those points within a vertical distance of 50 m from the data point are used to weight the point. The Sounding Generator produces a new sounding every 15 min.

In the end-state ITWS system, we envision both a full temperature field (in Cartesian coordinates) accompanying the ITWS Terminal Winds product [28], and a predictive column model for temperature, humidity, and winds. Either of these approaches should supersede the interim operational need for the Sounding Generator.

Data Preprocessing

The ITWS Microburst Prediction Algorithm receives the TDWR reflectivity data in radial form, which is the form in which the data are collected. The Data Preprocessing component maps these polar reflectivity data into three-dimensional Cartesian arrays and fills in missing data points. (Note: The TDWR elevation scans are not contiguous). These data are then passed directly to the Image Processing component of the ITWS Microburst Prediction Algorithm for analysis of microburst precursors. Simultaneously, the data are converted into two-dimensional maps of VIL, and these maps are passed to the ITWS Storm Motion Algorithm [29]. From these data, the Storm Motion Algorithm calculates an array of vectors representing the motion of VIL from the previous volume scan to the current scan. This vector array, which is also called the storm motion field, is then passed to the Image Processing component of the ITWS Microburst Prediction Algorithm.

The storm motion field is critical for all Image Processing feature detectors that compute changes in quantities (such as VIL) from one volume scan to the next. In such feature detectors, the storm motion field is used to advect the previous scan's data to the current time, and the advected image is subtracted from the current image to obtain the change in a certain



quantity (Figure 10). A misalignment in the two images caused, for example, by the motion field incorrectly representing the advection speed of the weather, can result in a significant degradation in the accuracy of the feature detectors.

Image Processing

To develop an algorithm for detecting gust fronts (the turbulent leading edges of thunderstorm outflows) from Doppler weather radar data, R.L. Delanoy and S.W. Troxel recently pioneered a fresh approach that uses techniques of data-level machine intelligence [19]. Their algorithm, developed at Lincoln Laboratory, has far exceeded the capabilities of previous algorithms for gust-front detection and, in some circumstances, the algorithm's performance has been comparable to that of human interpreters.

Delanoy and Troxel argued that the traditional algorithm design—characterized by a three-step process of detection, extraction or discrimination, and classification—leads to the loss of a significant amount of information at the outset and thus cannot be used to classify objects with ambiguous or weak signatures. When used at all in traditional algorithms, machine intelligence techniques were typically applied only in the final step, i.e., in the classification stage, when a great deal of underlying information had already been lost. In contrast, Delanoy and Troxel used machine intelligence techniques (e.g., knowledge-based signal processing, fuzzy-set theory, and pixel maps of *interest*) at the outset of processing, i.e., in the detection stage.

We used the philosophies and techniques of Delanoy and Troxel to develop the Image Processing component of the ITWS Microburst Prediction Algorithm. The prior algorithms based on machine-

FIGURE 9. Temperature data from (a) the National Meteorological Center (NMC) forecast model, (b) the MDCRS commercial-aircraft meteorological measurements and surface observations, (c) the result of the Sounding Generator combining data from parts a and b, and (d) the difference between the generated sounding of part c and the truth radiosonde temperature profile (the green curves in parts a, b, and c). These data were collected in Orlando on 5 August 1992 at 19:00 GMT. A special radiosonde balloon launch provided the truth dataset.

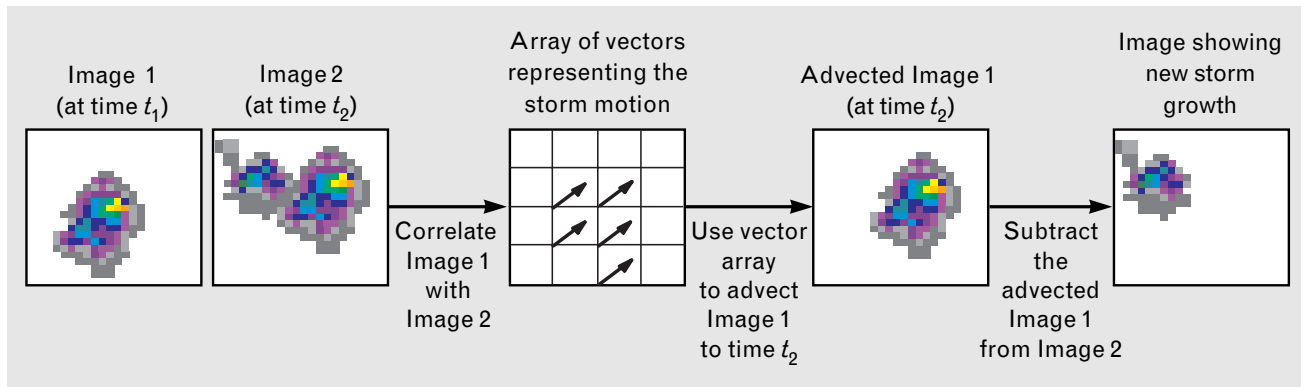


FIGURE 10. Example of how the Microburst Prediction Algorithm determines the change in a certain quantity (e.g., VIL) from one radar scan to the next. Two TDWR images at sequential times t_1 and t_2 are correlated by the ITWS Storm Motion Algorithm to determine the apparent storm motion from time t_1 to t_2 . This motion is represented by an array of vectors. With this vector array, the Microburst Prediction Algorithm advects the pixels in Image 1 to time t_2 , and then subtracts pixel by pixel the advected image from Image 2. The resulting image shows the area of new storm growth.

intelligence techniques, however, were detection-only algorithms whose only predictions were future locations of the object being detected on the basis of the object's current position and calculated motion. The added complication with our algorithm, which would have been a complication for any phenomenological prediction algorithm, is the need for an underlying model that describes how the detected object evolves in time. In our preliminary research (described earlier), we identified three stages of microburst evolution: growth, downdraft, and transition. These stages were used to define three categories of Image Processing feature detectors, namely, GROWTH, DOWNDRAFT, and TRANSITION, which are shown in Figure 11. Radar data from the 14 July 1994 Orlando microburst is shown at the top of the figure to illustrate the various stages of storm evolution.

Feature Detectors. The GROWTH feature detectors highlight regions where the condensed water in the atmosphere is increasing. There are three feature detectors for GROWTH:

1. RISE IN VIL—detects a rise in the VIL equivalent of reflectivity throughout the entire sample volume,
2. RISE IN VIF—detects a rise in the vertically integrated frozen water (VIF) equivalent of reflectivity (the quantity is integrated from the freezing level to the top of the sample volume), and
3. RISE IN FREEZING LEVEL VIL—detects a rise in

the VIL equivalent of reflectivity in a layer 3 km thick centered at the freezing level.

RISE IN VIF and RISE IN FREEZING LEVEL VIL aid RISE IN VIL by enabling a more focused capturing of early storm development. The three GROWTH feature detectors are combined with equal weights to construct an *interest image* of locations where the condensed water in the atmosphere is increasing.

The DOWNDRAFT feature detectors highlight regions where there are indications in the reflectivity field that the water load is beginning to descend and a downdraft is forming. There are two feature detectors for DOWNDRAFT:

1. DROP IN CENTER OF MASS—detects a drop in the altitude of the center of mass (CM) in regions where moderate VIL is present, and
2. DROP IN ECHO BOTTOM—detects a drop in the altitude of the echo bottom, i.e., the bottom of the reflectivity core, in regions where moderate VIL is present.

These two individual feature detectors are combined with equal weights to construct the combined DOWNDRAFT interest image.

The TRANSITION feature detector highlights regions that satisfy two conditions: downdraft has previously been indicated and weak yet increasing divergent wind shear is currently being detected. The TRANSITION feature detector uses wind-shear information from the ITWS Microburst Detection Algorithm. The wind-shear information is based

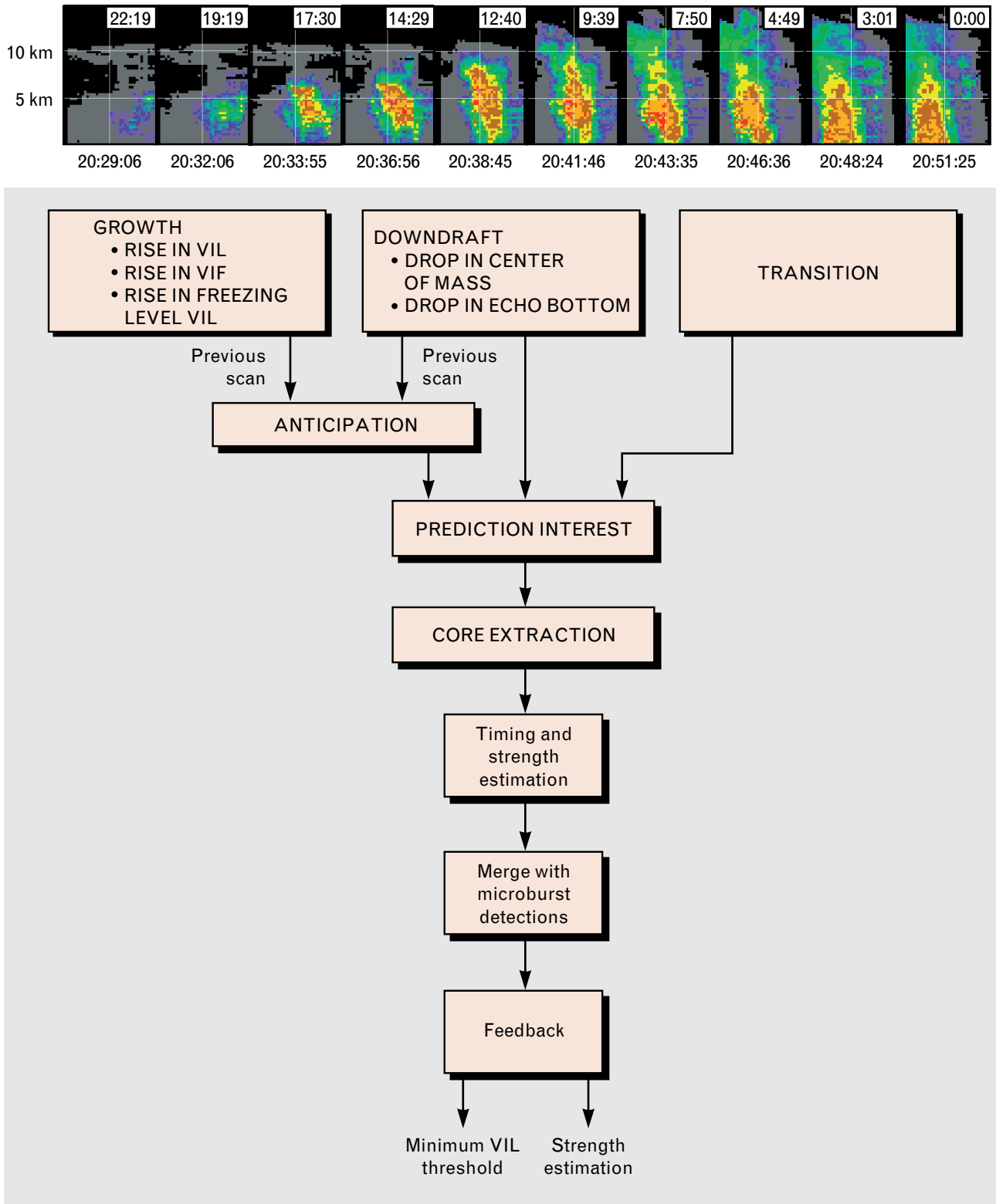


FIGURE 11. The Image Processing component of the Microburst Prediction Algorithm of Figure 8. Shown at the top of this figure are radar images, taken of the 14 July 1994 Orlando microburst, to illustrate the three stages of microburst evolution: growth, downdraft, and transition. These stages were used to define three categories of Image Processing feature detectors, namely, GROWTH, DOWNDRAFT, and TRANSITION.

on TDWR Doppler velocity data.

The GROWTH, DOWNDRAFT, and TRANSITION feature detectors all use *functional template correlation* [30, 31]—a knowledge-based signal processing technique—as a way of incorporating knowledge about the phenomena they are designed to detect. A functional template is a generalized matched filter that is applied to an image in much the same way that the subimage kernel is applied in autocorrelation. In functional template correlation, however, the kernel (or template) has an array of scoring functions, each of which returns a score indicating how well image values match expectations for each element of the kernel. The scoring functions return numerical values that are clipped to the continuous range [0, 1]. The final output is a *map of evidence*, which indicates the *interest* for the feature being detected. A high value of interest reflects greater confidence that the feature in question (e.g., a rise in the VIL level) is present at that location. Interest images from different feature detectors can be combined easily, thus providing a simple but powerful method of data fusion for data from disparate sources.

Figure 12 shows an example of the two functional templates that are used in the DROP IN CENTER OF MASS feature detector. The kernel shape (a square that is 3 pixels \times 3 pixels) is meant to represent a circular object, reflecting our expectation that thunderstorm cells will be roughly cylindrical in shape. In Figure 12(a), the scoring functions used to detect a drop in the center of mass give a full interest score of 1.0 to pixels with a drop in center of mass of 600 m or more from one scan to the next, and progressively less interest to smaller drops. Also, the scoring functions inhibit the interest values associated with rises in the center of mass, particularly at the center of the kernel, by returning negative interest scores for such cases. In Figure 12(b), other scoring functions are used simultaneously to inhibit indications of a drop in center of mass when only weak amounts of VIL are present, because weak VIL levels suggest that a downdraft might not be occurring even when there is a drop in the center of mass. Thus the VIL scoring functions strongly inhibit interest at weak VIL, and inhibit less as VIL increases to moderate levels. (The numerical values of VIL that indicate weak and moderate VIL

are determined from Equation 2 by using the estimated sounding for that day and time.) At higher VIL levels, the VIL scoring functions have no opinion, neither inhibiting nor accentuating the overall interest from the DROP IN CENTER OF MASS feature detector.

Anticipation. In Figure 11, one of the three sources of interest flowing into the PREDICTION INTEREST box is called ANTICIPATION. The ANTICIPATION interest image is derived from the maximum of the GROWTH and DOWNDRAFT interest on the previous volume scan. The ANTICIPATION image highlights the expected locations of microbursts. When the ANTICIPATION image is combined with the other interest images, it can support weak evidence that would otherwise be insufficient to trigger a prediction.

Combining Evidence. The PREDICTION INTEREST is computed by averaging the DOWNDRAFT interest image (with a weight of 0.75) and the ANTICIPATION interest image (with a weight of 0.25), and then choosing the maximum, on a pixel-by-pixel basis, of this average and the TRANSITION interest image. The weighting implies that GROWTH interest detected in the previous volume scan and/or DOWNDRAFT and TRANSITION interest in the current volume scan can trigger a microburst prediction. TRANSITION interest carries the most weight because it indicates that a weak outflow has already begun at the surface. Finally, to avoid predicting microbursts that are already in progress, we inhibit the combined interest image of PREDICTION INTEREST at locations where microbursts are currently being detected by the ITWS Microburst Detection Algorithm.

Extraction. Only in this final stage do we discard any data. In CORE EXTRACTION, a threshold of 0.5 is applied to the final interest image values, which range from 0.0 to 1.0. Any regions remaining above the 0.5 level are clustered and numbered as individual *cores*, i.e., areas likely to produce a microburst. In more traditional approaches to automated thunderstorm detection, this extraction step has been based solely on the measured reflectivity. By using interest images, we have highlighted regions of reflectivity that are all in a precursor phase to producing a surface outflow without the ambiguity of including thunderstorm regions that are in other phases of evolution. For these high-

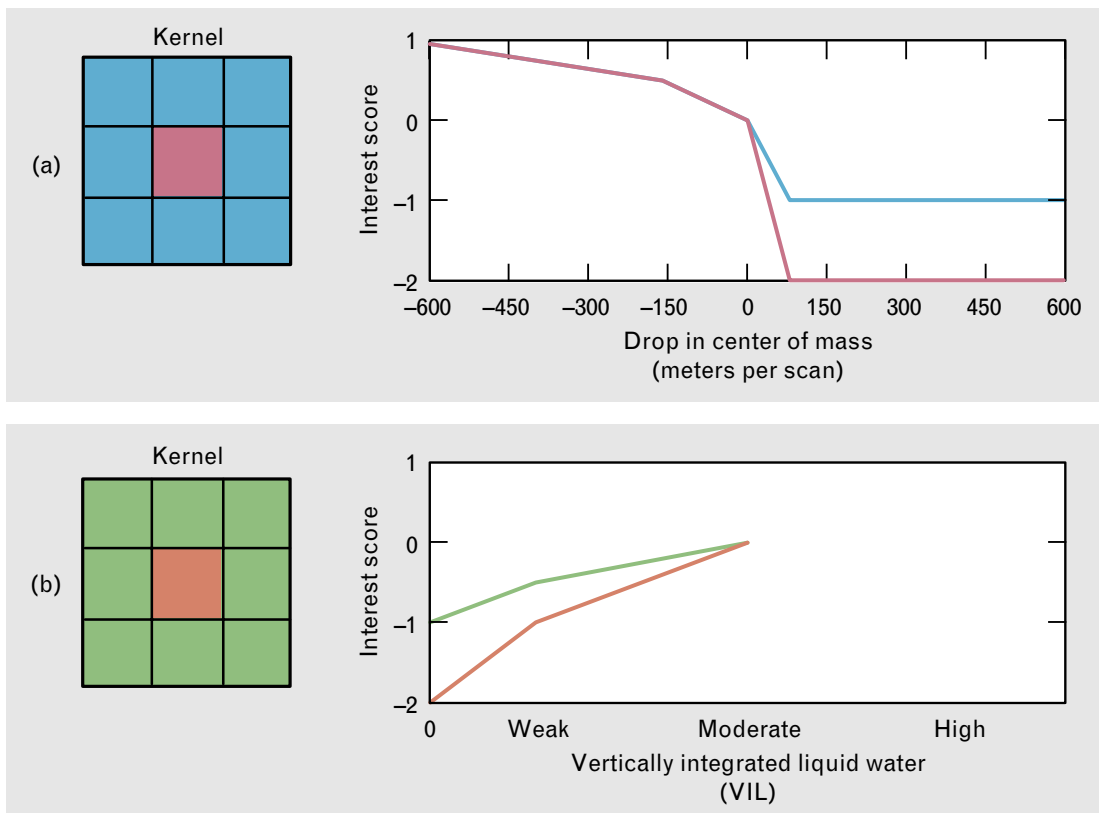


FIGURE 12. Example of the two functional templates used in the DROP IN CENTER OF MASS feature detector: (a) template used to score the drop in the center of mass, and (b) template used to take into account the VIL level. The left diagrams show the template kernels, which are placed on the radar imagery to look for certain storm characteristics, in this example, the presence of a downdraft. The right figures show the corresponding scoring functions, which are color coded to different locations in the kernels. Note that the scoring functions for the drop in center of mass give a full interest score of 1.0 to pixels with a drop in center of mass of 600 m or more from one scan to the next, and progressively less interest to smaller drops. Also, the scoring functions inhibit rises in the center of mass, particularly at the center of the kernel, by returning negative interest scores for such cases. Simultaneously, the VIL scoring functions are used to inhibit indications of a drop in the center of mass when only weak amounts of VIL are present.

lighted regions, Equation 2 is then applied by using the VIL present in the cores and the current sounding measurements. Only if the equation indicates an outflow strength greater than 30 kn (the threshold for a microburst) is a microburst prediction issued for the region.

Timing Estimation. In the final step before a prediction is issued, the timing of the microburst is estimated by a series of timing estimators using trends in the detected features and their relationships to each other. For example, Figure 13 illustrates the timing estimator that is based on RISE IN VIL and DROP IN CENTER OF MASS. We use a contingency table to indi-

cate the four possible relationships between these two feature detectors. When VIL is still rising and the storm CM has begun to drop, the table estimates that a microburst will occur (on average) in 7 min. If VIL is no longer rising and the storm CM is dropping, the microburst will occur (on average) in 4 min. The other two cases in the table are not indicative of microbursts; thus they have no timing estimate.

Example. Figure 14 shows the intermediate interest images in the prediction made for the 14 July 1994 Orlando microburst. At the top of the figure are the vertical cross sections showing the growth and subsequent decay of the reflectivity field of the microburst

parent storm. The first wind shear is detected at 20:48, 3 min prior to the onset of the microburst at 20:51 (last image in series). The GROWTH, DOWNDRAFT, and TRANSITION interest images are shown beneath the cross sections as gray-scale plots, with the brightest white pixels representing high interest at or near 1.0. The first GROWTH interest image plotted below the 20:32 reflectivity cross section represents the growth from the prior scan at 20:29 to the current scan at 20:32. The same is true of the DOWNDRAFT interest as well. The red circle in each interest image represents the location of the microburst at 20:51. The images in the last row are not interest images but maps of VIL plotted with a gray scale to indicate in two dimensions regions of high reflectivity. The blue circles in the last row of images represent predictions that the algorithm issued.

The GROWTH interest is very strong in the first four time frames. Also, note how the region of high interest moves from southeast to northwest. This motion is the storm advection, which can also be seen as a right-to-left motion in the reflectivity cross sections. In the last five GROWTH frames, new growth has begun in surrounding regions while little or no growth is taking place in the area of the microburst. The DOWNDRAFT interest is negligible until 20:38, when several high-interest pixels appear. The region of overlap of these interest values with that of GROWTH in the previous frame (20:36) produces a combined interest high enough to exceed ambiguity, thus producing a microburst prediction, i.e., a blue circle at 20:38. The timing estimates for this initial prediction and for the two following predictions were all 8 min, compared to the actual times of 12.7, 9.7, and 7.8 min. The DOWNDRAFT signal remains strong until 20:46, when the signal becomes more diffuse and other surrounding regions begin to show high interest levels. Note that the microburst prediction drops out at this point; i.e., there is no blue circle for 20:46. Nonetheless, because the timing estimate of the prediction on the previous scan has not yet expired, the prediction persists and there is no interruption on the end-user display. By the next volume scan (20:48), wind shear has begun at the ground surface, thus causing the TRANSITION feature detector to exhibit very high interest. TRANSITION renews and extends the microburst pre-

diction through the period when the downdraft has weakened but the wind shear at the ground surface has not yet reached microburst strength.

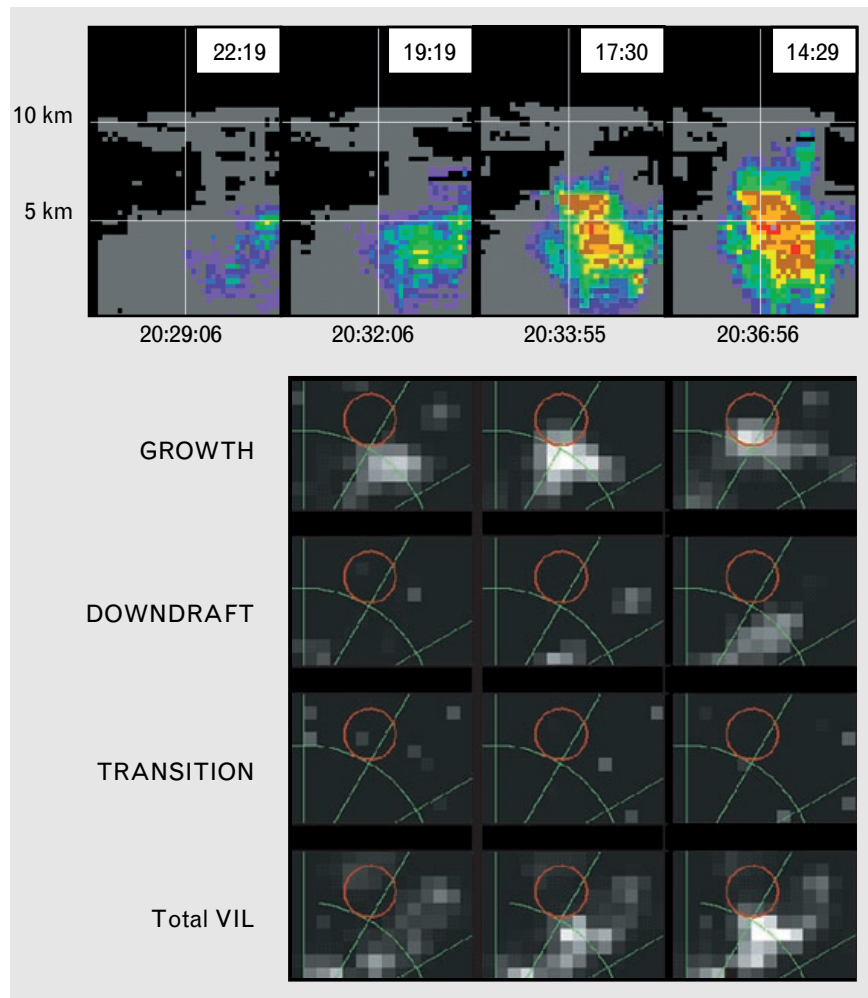
In the bottom row of VIL images, note how little the reflectivity changes after 20:38, i.e., once the primary storm growth has occurred. We can conclude that the total mass of the cell changes little during the very dynamic downdraft and transition phases of cell decay.

Feedback. One advantage of an integrated system such as ITWS that detects the very phenomenon being predicted is the opportunity to check the performance of the system automatically so that corrective feedback can be provided if the predictions are inaccurate. The feedback process in the ITWS Microburst Prediction Algorithm assesses performance in real time by comparing the algorithm's predictions with detections issued by the ITWS Microburst Detection Algorithm. At each feedback cycle (time t_0), predictions from time $t_0 - 20$ min to time $t_0 - 10$ min are compared with detections from time $t_0 - 10$ min to time t_0 . In the comparison process, the predictions and detections from their respective time periods are advected to the same time of $t_0 - 10$ min and the overlap is computed (Figure 15). The percent error is

		CM	
		Not dropping	Dropping
VIL	Not rising	Nil	4 min
	Rising	Nil	7 min

FIGURE 13. Contingency table for the timing estimator based on the feature detectors RISE IN VIL and DROP IN CENTER OF MASS. For the case in which VIL is still rising and the storm CM has begun to drop, the table estimates that a microburst will occur (on average) in 7 min. Note that a necessary condition for the occurrence of a microburst is that the storm CM must be dropping.

FIGURE 14. Combined output of the feature detectors GROWTH, DOWNDRAFT, and TRANSITION for the Orlando microburst on 14 July 1994. The vertical cross sections of TDWR reflectivity are shown at the top, and the gray-scale pixel images of interest are shown below. In the gray-scale images, brighter pixels indicate higher interest scores, and the red circles represent the locations of the final microburst outflow. Note that there is some propagation of the storm from southeast toward northwest. For reference purposes, the images in the last row are not interest images but maps of VIL plotted with a gray scale to indicate regions of high reflectivity. The blue circles in the bottom row represent predictions issued by the algorithm.



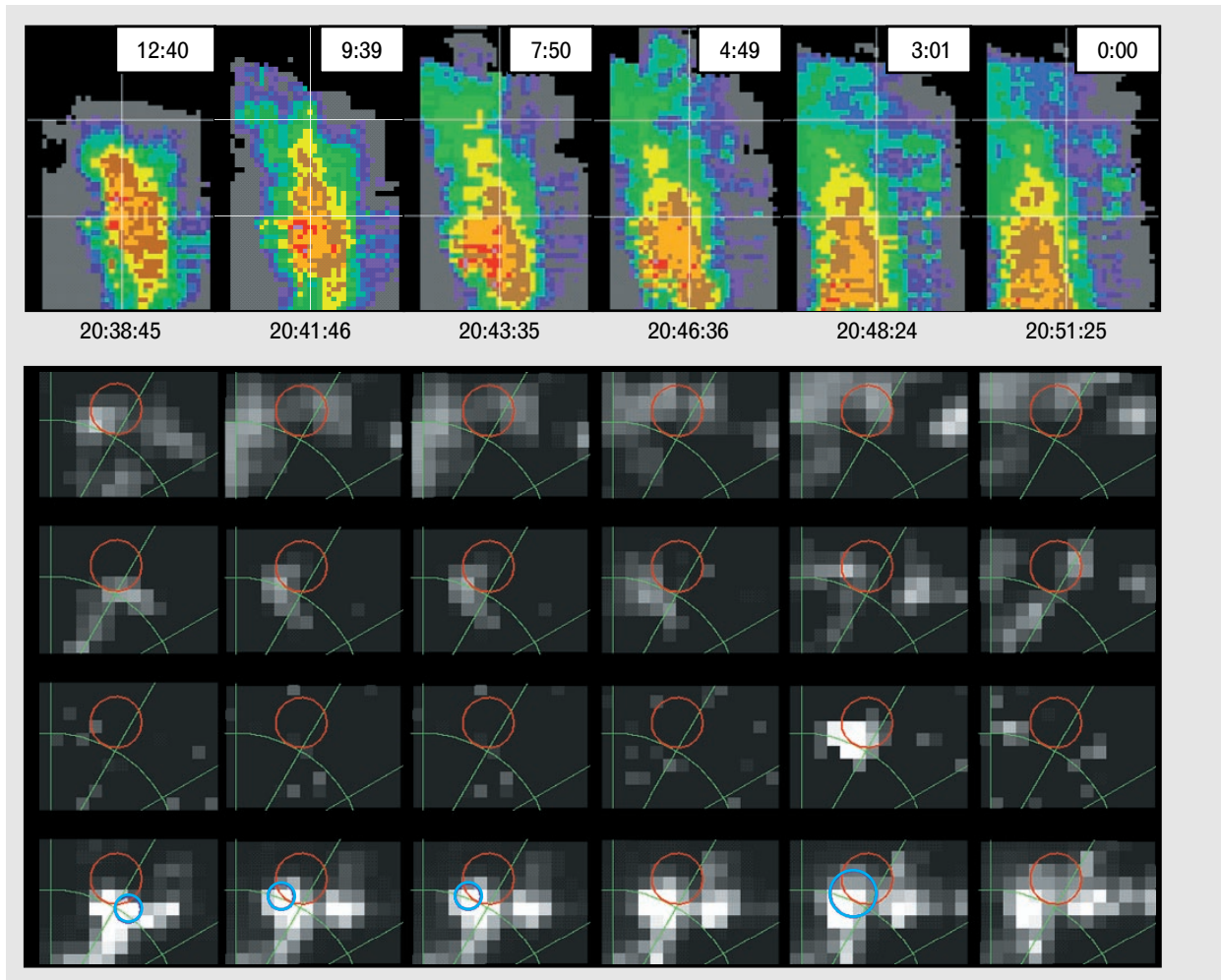
calculated from the strengths of the regions of detections but no predictions (indicating areas of underprediction), the regions of predictions but no detections (indicating areas of overprediction, or false alarms), and the regions where the predictions and detections overlapped. A new feedback cycle takes place every 10 min after an initial start-up time of 20 min.

If no microbursts were detected but predictions were made, then the system automatically desensitizes itself so that predictions become more difficult to issue in the future. On the other hand, if microbursts were detected but no predictions were made, then the system sensitizes itself so that predictions become easier to issue in the future. These adjustments are accomplished through a feedback coefficient (c_{fb} , in Equation 2) that is used to raise or lower slowly the amount of VIL needed for the system to predict a mi-

croburst. The coefficient c_{fb} depends on the percent error of the system and on other factors that force the coefficient to change at a faster rate either when there is high confidence that a change is needed or when the system is overpredicting because false alarms are very detrimental in an operational setting.

We have found that the feedback process can take a long time to become effective when the system is underpredicting. This situation occurred on days when there was very little VIL in the atmosphere and Equation 2 required a large amount of VIL to predict a microburst. In these cases a histogram of VIL can be used to obtain better approximations of the amount of VIL needed to predict a microburst, thus allowing the algorithm to begin issuing microburst predictions sooner. The feedback process can then be used to make the necessary small adjustments to the system.

The use of a feedback cycle is unique in the ITWS



system. When the sounding estimates are inaccurate, feedback provides a safety net for the algorithm. Because microbursts tend to occur in clusters with many microbursts occurring in a single day, the feedback process usually has enough information to minimize any inaccuracies in the sounding parameters. Through the use of feedback, the ITWS Microburst Prediction Algorithm eventually “learns” the correct environmental state, and the algorithm performance can actually be acceptable even if only a default sounding is available. Feedback, in addition to the use of thermodynamic data, obviates the need for site-adaptable parameters that are used to compensate for widely different climates and annual convective patterns.

Microburst Merge

The ITWS Microburst Prediction Algorithm was

originally envisioned as a planning product for supervisors and traffic managers. However, for the algorithm to be reliable with the current set of feature detectors and rules, a downdraft must be detected before the algorithm can issue a microburst prediction. This condition precludes the long lead times (greater than ten minutes) that are desired by air traffic planners for redirecting the flow of traffic to other runways. With the current algorithm, achievable lead times typically range from one to five minutes. Until additional operational experience in predicting microbursts has been obtained, air traffic users have requested that the information from the ITWS Microburst Prediction Algorithm be used to produce earlier warnings of microburst wind shear. This change would allow the safety-related information contained in the ITWS Microburst Prediction Algorithm to be utilized immediately in an operational

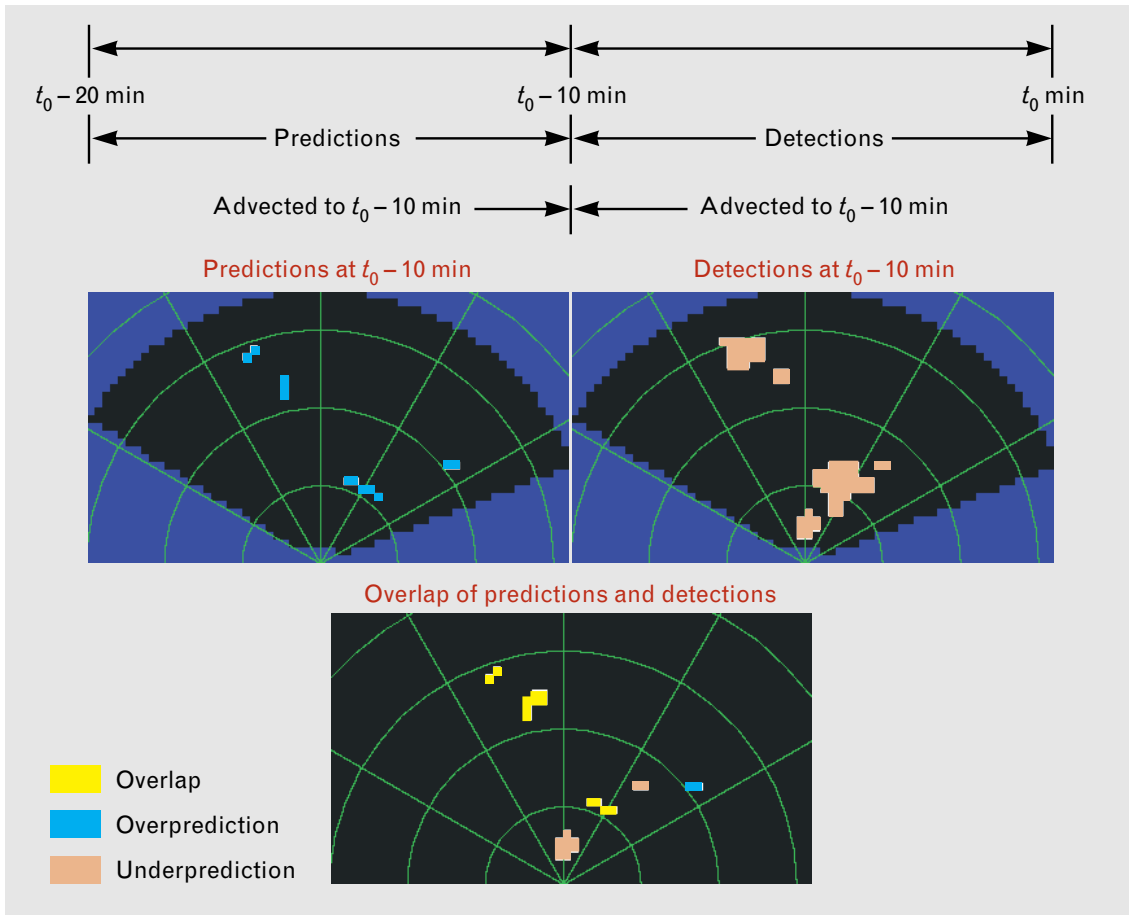


FIGURE 15. Diagram illustrating the feedback process used to compare microburst predictions with detections. In the process, predictions made in the period $t_0 - 20$ min to $t_0 - 10$ min are compared with the detections made in the period $t_0 - 10$ min to t_0 min. Both the predictions and detections are advected to time $t_0 - 10$ min before the overlap is computed. This example is for microbursts that occurred on 14 July 1994 in Orlando around 20:53 GMT. The range rings in the radar imagery are 10 km apart.

setting, and would reduce the time between the warning of microburst wind shear and the occurrence of that wind shear.

Microburst predictions are displayed on a Situation Display (SD) according to the following rules. If, when a microburst has been predicted, neither the TDWR nor the ITWS Microburst Detection Algorithm has issued a wind-shear alert (WSA), i.e., an alert for wind shear exceeding 15 kn, then the SD will display a circular 15-kn WSA, as shown in Figure 16(a). If, instead, one or more WSAs are already present, a microburst alert (MBA), i.e., an alert for wind shear exceeding 30 kn, will be issued on top of the WSA(s), as shown by the circular 30-kn MBA overlaid on the WSA in Figure 16(b). The sizes of the

circles used to indicate WSAs and MBAs delineate the regions of downdraft that the ITWS Microburst Prediction Algorithm has detected. These WSAs and MBAs are processed exactly as the TDWR microburst detections are processed, and they are reported on the controllers' ribbon display. This merging of microburst detections with predictions is performed by Microburst Merge, which is shown at the bottom of the block diagram in Figure 8.

Operational Display Concept

Figure 17 presents the data that were displayed operationally during the 14 July 1994 Orlando microburst discussed earlier. At 20:44, a 15-kn WSA was issued for the easternmost runway, to the north and just east

of the runway, as shown in Figure 17(a). Note that the SD has represented that runway and its approach path in red. The ribbon display message for pilots is shown below the SD image and is read as “Runway 17 approach: wind-shear alert; 15-kn loss; 1 mile final approach; winds at 120° at 8 kn.” At 20:48, actual wind shear of 15 kn was detected. Then the ITWS Microburst Prediction Algorithm upgraded the 15-kn WSA to a 30-kn MBA, as shown in Figure 17(b). Pilots were told “Runway 17 approach; microburst alert; 30-kn loss. . . .” At 20:51, the outflow had reached microburst strength and a 35-kn loss was reported on the runway, as shown in Figure 17(c). By 20:54, the microburst had reached its peak of 40 kn, as shown in Figure 17(d). Pilots using the runway received a WSA 3 to 4 min before they would have encountered the thunderstorm outflow, and an MBA 2 to 3 min before microburst-strength wind shear was present. The predictions in this case clearly provided a significant extra margin of safety.

Results

Over the past two years, there has been substantial progress in the development and refinement of the ITWS Microburst Prediction Algorithm. The operational concept has evolved so that the algorithm is now coupled with microburst detection to provide earlier microburst alerts when downdrafts, which are precursors to microburst outflows, have been detected. The ITWS Microburst Prediction Algorithm was tested in a real-time operational setting during the 1994 ITWS demonstration- and validation-phase operational test and evaluation (Dem/Val) at Memphis, Tennessee, and Orlando, Florida. The results from those tests are described in this section.

Because of its critical operational use, the ITWS Microburst Prediction Algorithm attempts to predict as many microbursts as possible while meeting a very strict false-alarm criterion. The stated ITWS functional requirement for the accuracy performance of the algorithm is summarized below:

Microburst prediction accuracy: ITWS shall be capable of a probability of correct prediction of microbursts (i.e., the actual loss ≥ 30 kn) of ≥ 0.30 in the terminal area. The probability that a prediction is false (i.e., the actual loss < 15 kn) shall be ≤ 0.10 .

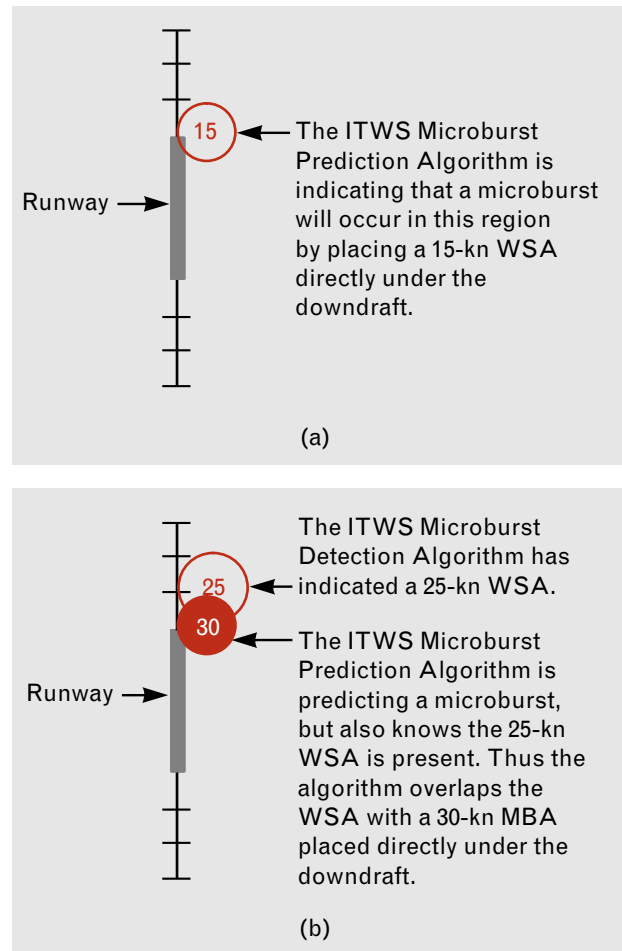


FIGURE 16. Figure illustrating the display concept for microburst predictions in two cases: (a) when a wind-shear alert (WSA) has not yet been issued, and (b) when a WSA has already been issued. Note that the microburst prediction is displayed as a 15-kn WSA in part a, and a 30-kn microburst alert (MBA) in part b.

This requirement states that, although it would be acceptable if the algorithm issues predictions for only 30% of the expected microburst events, the predictions that are issued must be accurate at least 90% of the time. This stipulation ensures that any issued predictions will be highly reliable.

Prior to the ITWS Dem/Val, our probability of false prediction (PFP) did not meet the above functional requirement on the Memphis test datasets. Thus we explored operating the system in a restricted mode and found that we could reduce the PFP by having the system wait until the ITWS Microburst Detection Algorithm had issued a true WSA before allowing the ITWS Microburst Prediction Algorithm

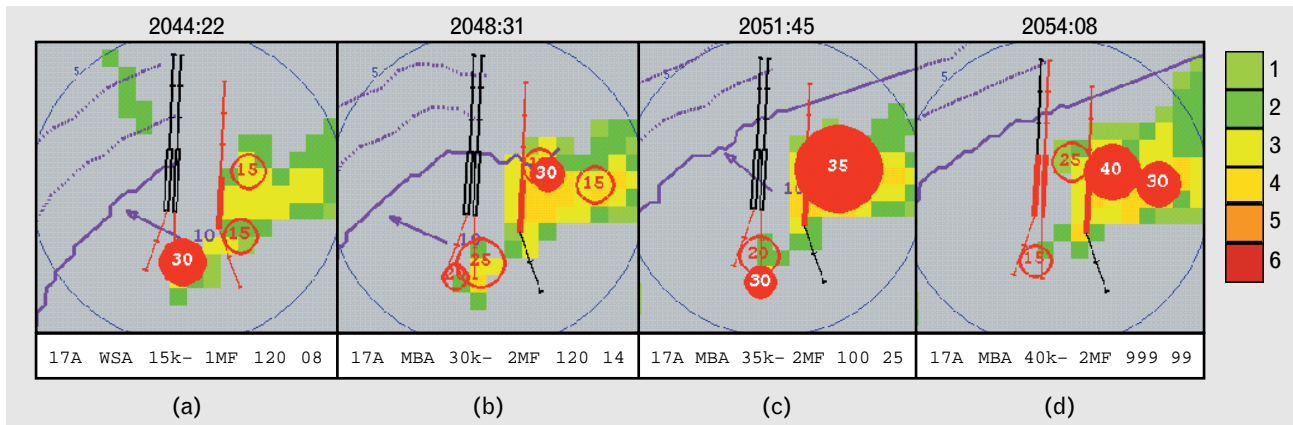


FIGURE 17. Time sequence of ITWS SD output for the 14 July 1994 microburst in Orlando: (a) a 15-kn WSA is issued for the easternmost (right-most) runway, to the north and just east of the runway, (b) because the system has detected a 15-kn wind shear, the 15-kn WSA has been upgraded to a 30-kn MBA, (c) the actual microburst detection is 35 kn over a large area, and (d) the peak strength reached by this microburst is 40 kn. Note that ribbon display messages are printed below the SD figures. For example, the message for part a is “Runway 17 approach; wind-shear alert; 15-kn loss; 1 mile final; winds at 120° and 8 kn.” The color bar at the right indicates the six NWS precipitation levels.

to take any action. By definition, this restriction reduces the PFP to zero (because wind shear with loss ≥ 15 kn must be present before the ITWS Microburst Prediction Algorithm can issue a microburst prediction), but it also reduces the number of microbursts predicted and decreases the lead time for those microbursts which are predicted.

A decision was made to run the Memphis Dem/Val in a restricted mode and the Orlando Dem/Val in an unrestricted mode. Table 2 shows the scoring results of both tests. For comparison purposes, the results were calculated for both the restricted and unrestricted modes at each site even though the system was run in only one of those modes. There were 25 microbursts in each dataset.

The probability of prediction (POP) was calculated by counting the number of events that the algorithm had predicted correctly and dividing that number by the total number of events that the algorithm should have predicted. An experienced meteorologist determined the total number of events that should have been predicted, and POP was calculated on an event-by-event basis. In determining the number of events that were predicted correctly, an analyst searched up to nine minutes ahead of each predicted microburst to find matching events. A prediction could be matched with only one event, but any given event could be matched with multiple predictions. If

an event was predicted at least once, the event was considered to be a correctly predicted event. Generally, we required a 25% overlap of the predicted and true regions. For very small alerts (less than 1-km radius), however, predictions within 1 km of the true events were also considered hits.

The probability of false prediction (PFP) was calculated by counting the number of false predictions issued by the algorithm and dividing that number by the total number of predictions issued. The PFP was calculated on a minute-by-minute basis by comparing the predictions issued with the detections made by the ITWS Microburst Detection Algorithm. In accordance with the PFP criterion in the ITWS functional requirements stated earlier, a false prediction was declared when the true loss was < 15 kn.

Table 2 shows that the POP comfortably exceeds the functional requirement of 30% at both sites, but that the required PFP of 10% cannot currently be achieved with the system running in an unrestricted mode. One obvious solution is to run the system in a restricted mode at all sites, but the reduction in lead time is substantial. At both the Memphis and Orlando sites, the majority of the false predictions were alarms that had been issued too late; i.e. the system predicted microbursts that, in actuality, were then decreasing after already having peaked. False predictions also occurred when the system had been run over-

night and the feedback cycle was operating with sounding information from the previous day. At Lincoln Laboratory, we are continuing research to address these and other shortcomings of the system. Our goal is to lower the PFP so that the algorithm can be utilized operationally in an unrestricted as well as restricted mode for providing warnings prior to the commencement of microburst outflow.

Summary

We have described the development of an algorithm that automatically and reliably predicts microburst wind shear. The algorithm, developed as part of the FAA Integrated Terminal Weather System (ITWS), is based on fundamental physical principles of thunderstorm evolution and downdraft development. The primary source of data for the algorithm is the Terminal Doppler Weather Radar (TDWR). To achieve high reliability, however, the algorithm also explicitly considers the atmospheric vertical temperature and humidity profile, data that will be available in automated systems such as ITWS.

Detailed research on thunderstorm dynamics has revealed the limitations of traditional methods for processing radar data. This research has been based on special triple-Doppler-radar processing, which permits highly accurate retrieval of the vertical velocity inside thunderstorms. From such research, we have rejected methods that first apply a threshold to the

reflectivity data to find storm *cells* and then follow these cells through their life cycles because such methods have proven to be error prone and often misleading when applied to the majority of microburst-producing storms.

Instead, we have used machine-intelligent image processing and data-fusion techniques to reveal those regions of growing thunderstorms (updrafts) and intensifying downdrafts which lead to microbursts. Derivatives of the reflectivity data are used to identify probable regions of downdraft, and these derivatives are combined with measures of the ambient temperature/humidity structure in the atmosphere to predict a microburst's location, timing, and outflow strength. The actual microburst detections are taken into account through a feedback cycle that compensates for any errors in the predictions. Such errors might be the result of, for example, inaccuracies in the estimated atmospheric sounding measurements or shortcomings in the underlying physical model for microburst development.

The ITWS Microburst Prediction Algorithm was tested in real time as part of the ITWS operational test and evaluation in 1994 at Memphis, Tennessee, and Orlando, Florida. The algorithm performed well with an average 72% probability of prediction, but the system had to be run in a restricted mode to meet the stated requirement for a probability of false prediction of less than 10%. The restricted mode re-

Table 2. Microburst Prediction Scoring Results for System Operating in the Unrestricted and Restricted Modes

	<i>Unrestricted Mode</i>			<i>Restricted Mode</i> ¹		
	<i>POP</i> ²	<i>PFP</i> ³	<i>Lead Time</i>	<i>POP</i> ²	<i>PFP</i> ³	<i>Lead Time</i>
Memphis	80%	33%	246 sec	80%	0%	126 sec
Orlando	64%	19%	205 sec	56%	0%	58 sec
Average	72%	27%	226 sec	68%	0%	92 sec

¹ In the restricted mode, the system must wait until the ITWS Microburst Detection Algorithm has issued a true WSA before allowing the ITWS Microburst Prediction Algorithm to take any action.
² Probability of prediction—calculated by counting the number of events that the system predicted correctly and dividing that number by the total number of events that the system should have predicted.
³ Probability of false prediction—calculated by counting the number of false predictions that the system issued and dividing that number by the total number of predictions issued.

duced both the average lead time (i.e., the average time between the issuance of a warning and the occurrence of microburst wind shear) from 3.8 to 1.5 min and the average probability of prediction from 72% to 68%. In future work, one goal will be to reduce the number of false alarms, which typically occur in stormy areas with wind shear that has previously reached microburst strength.

Future Work

The development of an automated algorithm for predicting microburst wind shear was a challenging endeavor. Future research and development for later phases of the ITWS program will involve, in part, the system's providing reliable predictions of the thunderstorms themselves in the terminal area. Predicting thunderstorms is apt to be even more difficult than predicting microbursts because the desired lead times, ranging from ten to thirty minutes or more, may require that a prediction of a storm in the terminal area be issued before any radar-detectable cloud growth has occurred. Much of the research and many of the elements used in developing the ITWS Microburst Prediction Algorithm will be useful for our future work in this area.

Acknowledgments

The authors thank Chris Keohan, Mark Isaming, Mike Matthews, Rich DeLaura, and Mike O'Donnell for their help in developing and testing the algorithm. The authors also acknowledge the help and support of Greg Salotollo at NTSB, the operators of the UND and MIT radars, the support personnel for the ITWS field testing, Bryce Courtney and Bob Curry for their help with the operational system concept, and Jim Evans, David Sankey, and Ken Klasinski for their program management.

REFERENCES

1. National Research Council, *Low-Altitude Wind Shear and Its Hazard to Aviation* (National Academy Press, Washington, DC, 1983).
2. T.T. Fujita, *The Downburst* (University of Chicago, Dept. of Geophysical Sciences, 1985).
3. J.W. Wilson, R.D. Roberts, C. Kessinger, and J. McCarthy, "Microburst Wind Structure and Evaluation of Doppler Radar for Wind Shear Detection," *J. Climate Appl. Meteor.* **23**, 898 (1984).
4. J.E. Evans and D. Turnbull, "Development of an Automated Windshear Detection System Using Doppler Weather Radar," *Proc. IEEE* **77**, 1661 (1989).
5. M.W. Merritt, D. Klinge-Wilson, and S.D. Campbell, "Wind Shear Detection with Pencil-Beam Radars," *Linc. Lab. J.* **2**, 483 (1989).
6. J.E. Evans and D.M. Bernella, "Supporting the Deployment of the Terminal Doppler Weather Radar (TDWR)," *Linc. Lab. J.*, in this issue.
7. J.E. Evans and E.R. Ducot, "The Integrated Terminal Weather System (ITWS)," *Linc. Lab. J.*, in this issue.
8. M.M. Wolfson, "Characteristics of Microbursts in the Continental United States," *Linc. Lab. J.* **1**, 49 (1988).
9. P.J. Biron and M.A. Isaming, "An Analysis of Microburst Characteristics Related to Automatic Detection from Huntsville, AL and Denver, CO," *Preprints, 24th Conf. on Radar Meteorology, Tallahassee, FL, 27-31 Mar. 1989*, American Meteorological Society, p. 269.
10. M.M. Wolfson, D. Klinge-Wilson, M.F. Donovan, J.A. Cullen, D.R. Neilley, M.C. Liepins, R.G. Hallowell, J.D. DiStefano, D.A. Clark, M.A. Isaming, P.J. Biron, and B.E. Forman, "Characteristics of Thunderstorm-Generated Low Altitude Wind Shear: A Survey Based on Nationwide Terminal Doppler Weather Radar Testbed Measurements," *Preprints, 29th IEEE Conf. on Decision and Control*, p. 682 (1990).
11. C.F. Keohan, M.C. Liepins, C.A. Meuse, and M.M. Wolfson, "Summary of Triple Doppler Data, Orlando 1991," *Project Report ATC-186*, MIT Lincoln Laboratory (7 Apr. 1992), DOT/FAA/NR-92/2.
12. R. DeLaura, M.M. Wolfson, and P.S. Ray, "A Hybrid Cartesian Synthesis Technique Using Triple Doppler Radar Networks," *Preprints, 25th Int. Conf. on Radar Meteorology, Paris, 24-28 June 1991*, American Meteorological Society, p. 630.
13. H.R. Byers and R.R. Braham, Jr., *The Thunderstorm* (U.S. Department of Commerce, Washington, DC, 1949).
14. R.K. Crane, "Automatic Cell Detection and Tracking," *IEEE Trans. Geosci. Electron.* **GE-17**, 250 (1979).
15. J.G. Wieler, F.I. Harris, and M.R. Snapp, "An Evaluation of an Automatic Cell Detection and Tracking Algorithm," Air Force Geophysics Laboratory, AFGL-TR-0368 (1982).

16. M. Dixon and G. Wiener, "TITAN: Thunderstorm Identification, Tracking, Analysis, and Nowcasting—A Radar Based Methodology," *J. Atmos. Ocean. Technol.* **10**, 785 (1993).
17. A. Witt and J.T. Johnson, "An Enhanced Storm Cell Identification and Tracking Algorithm," *Preprints, 26th Int. Conf. on Radar Meteorology, Norman, OK, 24–28 May 1993*, American Meteorological Society, p. 141.
18. R.L. Delanoy, J.G. Verly, and D.E. Dudgeon, "Machine Intelligent Automatic Recognition of Critical Mobile Targets in Laser Radar Imagery," *Linc. Lab. J.* **6**, 161 (1993).
19. R.L. Delanoy and S.W. Troxel, "Machine Intelligent Gust Front Detection," *Linc. Lab. J.* **6**, 187 (1993).
20. S.D. Campbell, "Microburst Precursor Recognition Using an Expert System Approach," *Preprints, 4th Int. Conf. on Interactive Information and Processing Systems for Meteorology, Oceanography and Hydrology*, American Meteorological Society, p. 300 (1989).
21. M.M. Wolfson, "Understanding and Predicting Microbursts," *Preprints, 16th Conf. on Severe Local Storms, Alberta, Canada, 22–26 Oct. 1990*, American Meteorological Society, p. 340.
22. F.H. Proctor, "Numerical Simulations of an Isolated Microburst. Part II: Sensitivity Experiments," *J. Atmos. Sci.* **46**, 2143 (1989).
23. K.K. Droegemeier, "A Multi-Parameter Study of Numerically-Simulated Microbursts for Use in Developing an Expert System for the Honeywell Windshear Computer," Final Report, contract nos. T114732L and T114733L (School of Meteorology, University of Oklahoma, Norman, OK, 1992).
24. S.G. Benjamin, K.J. Brundage, and L.L. Morone, "The Rapid Update Cycle. Part I: Analysis/Model Description," *NWS Technical Procedures Bulletin No. 416* (1994).
25. R.C. Martin, M.M. Wolfson, and R.G. Hallowell, "MDCRS: Aircraft Observations Collection and Uses," *Preprints, 5th Int. Conf. on Aviation Weather Systems, Vienna, VA*, p. 317 (1993).
26. S.G. Benjamin, K.A. Brewster, R. Brümmer, B.F. Jewett, T.W. Schlatter, T.L. Smith, and P.A. Stamus, "An Isentropic Three-Hourly Data Assimilation System Using ACARS Observations," *Mon. Weather Rev.*, **119**, 888 (1991).
27. R.J. Fleming and A.J. Hills, "Humidity Profiles via Commercial Aircraft," *8th Symp. of Meteorological Observations and Instrumentation, 17–22 Jan. 1993, Anaheim, CA*, American Meteorological Society (1993).
28. R.E. Cole and F.W. Wilson, "The Integrated Terminal Weather System Terminal Winds Product," *Linc. Lab. J.*, in this issue.
29. E.S. Chornoboy, A.M. Matlin, and J.P. Morgan, "Automated Storm Tracking for Terminal Air Traffic Control," *Linc. Lab. J.*, in this issue.
30. R.L. Delanoy, J.G. Verly, and D.E. Dudgeon, "Functional Templates and Their Application to 3-D Object Recognition," *Proc. Int. Conf. on Acoustics, Speech, and Signal Processing (ICAASP) 3*, San Francisco, 23–26 Mar. 1992, p. 141.
31. R.L. Delanoy, J.G. Verly, and D.E. Dudgeon, "Pixel-Level Fusion Using Interest Images," *Technical Report 979*, MIT Lincoln Laboratory (26 Apr. 1993).



Coauthors (left to right) Richard L. Delanoy, Margita L. Pawlak, Robert G. Hallowell, Marilyn M. Wolfson, Barbara E. Forman, and Peter D. Smith.

MARILYN M. WOLFSON received a B.S. degree in atmospheric and oceanic science in 1979 from the University of Michigan College of Engineering, where she was the recipient of the Outstanding Achievement Award for Atmospheric Sciences. She participated in the first NASA Summer Institute on Planetary Atmospheres and Climate at Goddard Institute for Space Studies in New York. She received her S.M. degree in 1983 from MIT, where she was awarded an Ida M. Green Graduate Fellowship, and she completed her Ph.D. degree at MIT in 1990 as a Lincoln Laboratory staff associate.

Marilyn is currently a staff member in the Weather Sensing Group, where she has performed applied meteorological studies related to the aviation avoidance of hazardous weather. She has written several articles and reports that have appeared in meteorological journals, conference proceedings, and Lincoln Laboratory publications.

Marilyn is currently a member of two National Research Council Committees: the National Weather Service Modernization Committee (NWSMC), which was established by the National Oceanic

and Atmospheric Administration (NOAA) to review the modernization and associated restructuring of the National Weather Service (NWS); and the Committee on Meteorological Analysis, Prediction, and Research (CMAPR), which is one of four standing committees of the Board on Atmospheric Sciences and Climate and the principal advisory group to the federal government for research and operations in dynamical, physical, synoptic, and applied meteorology.

In 1994, Marilyn received the American Meteorological Society Editor's Award for her work as an associate editor of *Monthly Weather Review*. She is a member of the American Meteorological Society, Sigma Xi, and Tau Beta Pi. Her outside interests include naturopathic and allopathic medicine, and she is an avid "reader" of books on tape.

RICHARD L. DELANOY is a staff member in the Machine Intelligence Technology Group. His work spans the fields of computer vision, machine learning, and the construction of object-recognition systems. From 1980 to 1983, he was a research scientist at the University of Virgin-

ia Department of Psychology, where he investigated the biochemical correlates of learning and the effects of stress-related hormones on electrophysiological models of memory. Before joining Lincoln Laboratory in 1987, he worked for GE Fanuc Automation N.A., Inc., as a software engineer developing numerical and programmable controllers for manufacturing automation.

Dick received a B.A. degree in biology from Wake Forest University in 1973, a Ph.D. degree in neuroscience from the University of Florida College of Medicine in 1979, and an M.S. degree in computer science from the University of Virginia in 1987. He was a National Science Foundation Predoctoral Fellow and a National Institute of Mental Health Postdoctoral Fellow.

BARBARA E. FORMAN is an assistant staff member in the Weather Sensing Group, where her focus of research has been on the aviation avoidance of hazardous weather. Before joining Lincoln Laboratory, Barbara worked for Bell Laboratories. She received a B.S. degree in mathematics from Simmons College, and is currently pursuing an M.S. degree in computer science from Boston University. Barbara's outside interests include tennis, reading, and bridge.

ROBERT G. HALLOWELL is an assistant staff member in the Weather Sensing Group, where his focus of research has been on the aviation avoidance of hazardous weather. Before joining Lincoln Laboratory eight years ago, he worked for Camp, Dresser and McKee, Inc., an environmental consulting firm in Boston. Bob received a B.S. degree in meteorology from the University of Lowell. In his free time, he enjoys politics, antique toys, and coin collecting.

MARGITA L. PAWLAK is an assistant staff member in

the Weather Sensing Group, where her focus of research has been on the aviation avoidance of hazardous weather. Margo received a B.S. degree in mathematics from the University of New Hampshire. Her outside interests include hiking, biking, and skiing.

PETER D. SMITH is a technical assistant in the Weather Sensing Group, where he has worked on the development of the ITWS Microburst Prediction Algorithm. Before joining Lincoln Laboratory three years ago, he worked for the University of Lowell Research Foundation. Peter received a B.S. degree in meteorology from the University of Lowell.